10
9/20/96 gsd

ERNEST ORLANDO LAWRENCE
BERKELEY NATIONAL LABORATORY

Energy & Environment Division

Energy Conversion & Storage Program

1995 Annual Report

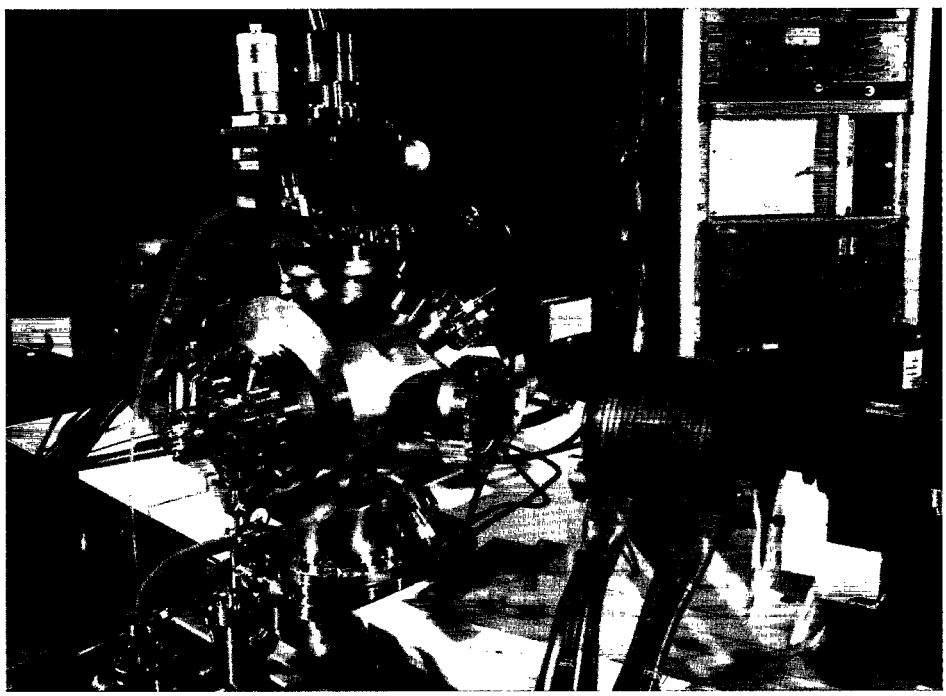

June 1996

LBL-38350
UC-1600

Cover: Spectroscopic ellipsometer and vacuum chamber, used to characterize the products of reactions between metallic lithium and components of battery electrolytes.

Available to DOE and DOE Contractors from
Office of Scientific and Technical Information
P.O. Box 62, Oak Ridge, TN 37831
Prices available from (615) 576-8401

Available to the public from
National Technical Information Service
U.S. Department of Commerce
5285 Port Royal Road, Springfield, VA 22161

Prepared for the U.S. Department of Energy under Contract No. DE-AC03-76SF00098

Energy Conversion & Storage Program 1995 Annual Report

Elton J. Cairns, Program Head

Energy & Environment Division
Ernest Orlando Lawrence Berkeley National Laboratory
University of California
Berkeley, California 94720
(510) 486-5001

Report No. LBL-38350

Contents

Introduction

The Energy Conversion and Storage (EC&S) Program investigates state-of-the-art electrochemistry, chemistry, and materials science technologies for:

- development of high-performance rechargeable batteries and fuel cells;
- development of high-efficiency thermochemical processes for energy conversion;
- characterization of new chemical processes and complex chemical species;
- study and application of novel materials related to energy conversion and transmission.

Research projects focus on transport-process principles, chemical kinetics, thermodynamics, separation processes, organic and physical chemistry, novel materials and deposition technologies, and advanced methods of analysis.

Electrochemistry research aims to develop advanced power systems for electric vehicle and other energy storage applications. Phenomenological and modeling studies are conducted to elucidate fundamental electrochemical processes. Advanced spectroscopic and traditional electrochemical characterization methods are used to study new electrochemical systems. Topics include the exploratory development of new electrochemical couples for advanced rechargeable batteries, improvements in battery and fuel-cell materials, the establishment of engineering principles applicable to electrochemical energy storage and conversion, and the characterization of advanced high-performance cells in collaboration with industry. LBNL-EED-EC&S is the designated Lead Center for management of the Exploratory Technology Research (ETR) Program, designed to identify new components for advanced batteries and fuel cells, with major emphasis on applied research that will lead to superior performance and lower life-cycle costs.

Chemical Applications research includes topics such as separations, catalysis, fuels, and chemical analyses. Included in this program area are projects to develop improved, energy efficient methods for processing product and waste streams, coal gasifiers, and biomass conversion processes. The development of reliable new methods for removing solids and gaseous contaminants from coal-gas at high temperatures and pressures is one of the most important technological advances required in the field of coal gasification. Reversible chemical complexation is investigated for selective separations of compounds from formation media for product recovery. The use of polymer pendant organic ligands is investigated as an efficient technology for the removal and recovery of toxic metal ions from waste streams. Extended x-ray absorption fine structure (EXAFS) is combined with electrochemical processes to obtain a thorough understanding of the lithium intercalation processes on an atomic level. Laser material-interactions are being investigated for sensitive chemical analyses of environmental and waste-stream species.

Materials Applications research includes the evaluation of the properties of advanced materials, as well as the development of novel preparation techniques. Pulsed laser deposition is being used to produce high temperature superconducting thin films and new rechargeable battery electrode materials. Sol-gel and solvent extraction methods are used to produce aerogel superinsulators; and light scattering techniques are being adapted to characterize sea water and sea ice in order to better interpret remote observations of the surface of the earth.

Program Staff

Elton J. Cairns, *Program Head*

Thomas Adler
Michael Ayers
Paul Berdahl
Edério Bidóia
Harvey Blanch
Robert Broekhuis
Mark Brooks
Garth Burns
Manuel Caetano
Van Carey
Hong Chen
Jie Chen
Yufei Chen
Daniel Chinn
Yohan Choi
Xi Chu
Douglas Clark
Christopher Coen
Stephen Cramer
Robert Darling
Charles Deng
Zhongyi Deng
Liliane DeSouza
Joszef Devenyi
Thomas Devine
Marc Doyle
Eve Edelson
L. Erskine
Laurent Fenouil
Richard Fish
Dania Ghantous
Melissa Grush
Craig Horne
Song-Ping Huang
Arlon Hunt
Mary Hunt
Scott Husson
Sungho Jeong
Jordan Kahn
John Kerr
Marvin Kilgo
Kim Kinoshita
Fanping Kong
Robert Kostecki
Henry Kuo
Chun-Pong Lau
Susan Lauer
Wei Li
Scott Lynn
Xianglei Mao
Diana Marmorstein
Frank McLarnon
Jeremy Meyers
David Miller
Jeffrey Moore
John Newman
Seiji Ogo
Blaine Paxton
Michael Perry
Bavanethan Pillay
Kathryn Podolske
Alain Rabion
Clayton Randall
Lin Rao
Ronald Reade
John Rheaume
Paul Ridgway
Diedra Rolland
James Rudnicki
Benjamin Rush
Richard Russo
Werner Schnurnberger
Robert Selleck
Mark Shannon
Xiangyun Song
Jonathan Spear
Charlotte Standish
Peter Stevens
Kathryn Striebel
Minmin Tian
Jerome Thomas
Jan van Elp
Hongxin Wang
Xiaodong Wang
Jue Wang
Xin Wang
Shi-Jie Wen
Charles Wilkes
Mark Yahnke
Shouquan Zeng

Electrochemistry

Exploratory Technology Research Program for Electrochemical Energy Storage

K. Kinoshita, F.R. McLarnon, and E.J. Cairns

Lawrence Berkeley National Laboratory (LBNL) is lead center for management of the Exploratory Technology Research (ETR) Program, which is supported by the Electric/Hybrid Propulsion Division of DOE's Office of Transportation Technologies. This program's research supports DOE development of electrochemical energy conversion systems for potential use in electric vehicles. The most promising electrochemical technologies are identified and transferred to the U.S Advanced Battery Consortium (USABC) and/or to another DOE program for further development and scale-up.

The ETR Program identifies new electrochemical couples for advanced batteries, determines the technical feasibility of the new couples, improves battery components and materials, establishes engineering principles applicable to electrochemical energy storage and conversion, and investigates fuel cell and metal/air systems for transportation applications. Major emphasis is given to applied research that will lead to superior performance and lower life-cycle costs.

The LBNL senior investigators participating in the project are E.J. Cairns, J.W. Evans, K. Kinoshita, F.R. McLarnon, J.S. Newman and C.W. Tobias* (emeritus professor) of the Energy and Environment Division; and L.C. DeJonghe and P.N. Ross of the Materials Sciences Division. Research projects conducted by subcontractors are described in the recent annual report, Exploratory Technology Research Program for Electrochemical Energy Storage (LBL-37665). Highlights of the ETR Program subcontracted work follow.

Exploratory Research

Oak Ridge National Laboratory (ORNL) has fabricated all-solid-state Li/$Li_xMn_2O_4$ cells that exhibited good performance with less than 0.05% capacity loss per cycle after hundreds of cycles when discharged at 20–40 mA/cm² to 2–3 volts (~C/1). Efforts are underway to fabricate thicker Mn oxide electrodes to improve the specific energy of the cell.

Georgia Institute of Technology has achieved sodium plating and stripping with 94% coulombic efficiency at current densities to 25 mA/cm² in an electrolyte that contains methyl-ethyl imidazolium chloride/aluminum chloride buffered with sodium chloride.

PolyPlus Battery Co. achieved 20 cycles at 100 Wh/kg with Na/organosulfur (Na/SRPE) cells at 90°C. The Na electrode was prone to shorting during the charge cycles, and this charging instability is attributed to the difficulty in maintaining a contamination-free Na/polyethylene oxide (PEO) interface.

Applied Science Research

Several projects are underway that utilize advanced spectroscopic techniques to investigate cell components or phenomena that occur during cell operation. Brookhaven National Laboratory (BNL) has used extended X-ray absorption fine structure (EXAFS) and X-ray absorption near-edge spectroscopy (XANES) to study nickel oxide electrodes that were cycled in Zn/NiOOH cells. EXAFS showed no specific interaction of the zincate with $Ni(OH)_2$. Ni EXAFS for a nickel oxide electrode (with sintered plaque) after cycling indicate that most of the sintered plaque had corroded to form β-$Ni(OH)_2$. Southern University is also investigating the applicability of EXAFS *in situ* studies of Li/FeS_2 cells. An electrochemical system for the *in situ* studies has been fabricated. Case Western Reserve University (CWRU) designed and constructed a versatile variable-temperature electrochemical cell for conducting *in situ* attenuated total reflection-Fourier transform infrared spectroscopic (ATR-FTIR) experiments under reduced pressure. The results with Li/PEO($LiAsF_6$) suggest that under the experimental conditions selected for these studies, and to the level of sensitivity of this technique, PEO($LiAsF_6$) does not react with metallic Li.

Projects are underway to identify improved polymer electrolytes and to understand transport phenomena which will guide the development effort. Northwestern University (NWU) has synthesized polymer electrolytes based on aluminosilicate-polyether hybrid electrolytes, (amorphous PEO)$_{25}$LiTf and (amorphous PEO)$_{38}$Li[Al(OSiEt$_3$)$_4$], which yielded 135 mAh/g active cathode material in Li/$Li_xMn_2O_4$ cells. In another project, NWU showed conclusively by molecular dynamics simulation that in polymer/salt electrolytes of the stoichiometry usually measured, there are very few free ions, and that the conductivity is fixed both by the segmental relaxation of the polymer host (the renewal time) and by the number of effectively free ions. The University of Dayton has successfully prepared a novel liquid crystalline monomer, 4-[11-acryloylundecan-1yl)oxy]-4'-(4'-carboxybenzo-15-crown-5)biphenyl (ACB), by a four-step synthetic route. Studies are underway to prepare aligned, doped polymeric films with ACB that contain crown ethers which could have a fundamentally different mode of ion transport than those currently under investigation. CWRU also successfully sulfonated a polybenzimidazole (PBI) to obtain 2.1 to 2.2 sulfonic acid groups per PBI unit.

Lawrence Livermore National Laboratory (LLNL) observed that electrodes fabricated from various Lonza graphites yielded Li intercalation capacities that range from 320 to 365 mAh/g (equivalent to x in Li_xC_6 from 0.85 to 0.95), approaching the theoretical value of 372 mAh/g corresponding to LiC_6. The graphite powders with particle diameter in the range of 6-44 mm showed no Li diffusion limitation to deintercalation at rates from C/2 to C/60.

The State University of New York (Binghamton) has produced hexagonal Mo oxides by a hydrothermal method at 150-200°C which has a greater capacity for Li intercalation than the normal MoO_3

*deceased 1996

phase.

The Environmental Research Institute of Michigan (ERIM) has prepared TiN-coated Al containment materials, and two cells using these coatings produced by commercial reactive ion-plating have achieved over 300 cycles on accelerated charge/discharge cycles (at a rate of ~2/day) at Silent Power Ltd., Salt Lake City, UT.

Rutgers University has completed a project which identified alumina-containing formulations that showed improved thermodynamic stability. A formulation containing 14 mol% alumina had the highest ionic conductivity of 4.7×10^{-6} S/cm at 250°C.

SRI International cycled a Na/PEO_8NaTf/polyorganopolydisulfide (polyHTB) cell and achieved a cathode utilization of 164 mAh/g, with a specific energy of 260 Wh/kg (C/10 rate) at 95°C.

Air Systems Research

Eltech Research Corporation completed a project on bifunctional air electrodes. They achieved 145 cycles with electrodes containing graphitized carbon black (Monarch 120) for the support and $La_{0.6}Ca_{0.4}CoO_3$ as electrocatalysts in 35 wt% KOH at room temperature.

Los Alamos National Laboratory (LANL) obtained for the first time, limiting currents significantly in excess of 2 A/cm² in H_2/air proton-exchange membrane (PEM) fuel cells under ordinary operating conditions. Nuclear magnetic resonance (NMR) was used to show that the diffusion coefficient of methanol in Nafion membranes is only a factor of 2–3 smaller than in aqueous solutions, and this is an important factor contributing to the sizable cross-over rates observed with methanol. LANL has experimentally established that with a cathode of low Pt loading (0.4 mg/cm²), the cathode loss caused by methanol cross-over could easily reach 100 mV.

Future Directions

New projects were initiated with Brookhaven National Laboratory, University of South Carolina and University of Michigan on metal/hydride batteries, and the University of Wisconsin and SAFT America, Inc. on double-layer capacitors. These projects were selected from the submissions received from a Request-for-Proposal issued by LBL on "Applied Research on Novel Cell Components for Advanced Secondary Batteries and Capacitors."

References

Kinoshita K, *et al. Exploratory Technology Research Program for Electrochemical Energy Storage: Annual Report for 1994.* Lawrence Berkeley National Laboratory Report No. LBL-37665 (September 1995).

McLarnon F. Exploratory Technology Program for Electrochemical Energy Storage. In: *Proc. Annual Automotive Technology Development Contractors' Coordination Meeting, 1994.* Vol. P-289. Warrendale, PA: Society of Automotive Engineers, 1995, p. 211.

Klein M and McLarnon F. Nickel-Zinc Batteries. Chap. 29. In: *Handbook of Batteries.* 2nd Edition. D. Linden, ed. New York: McGraw-Hill Book Co., 1995, p. 29.1.

Advanced Electrode Research

E.J. Cairns, F.R. McLarnon, T.C. Adler, E. Bidóia, D. Marmorstein, M.L. Perry, J.A. Reimer**, B. Rush, W. Schnurnberger*, and M.S. Yahnke*

We have been studying the behavior of electrodes used in advanced secondary batteries and fuel cells currently under development for energy storage applications such as electric vehicles. We have also continued to investigate practical means for improving the performance and lifetimes of these batteries and fuel cells. Systems of current interest include the metal-hydride/nickel oxide battery; nonaqueous-electrolyte cells with Li electrodes (Li/polymer, Li-ion); and fuel cells that utilize the direct electrooxidation of methanol. We study life-limiting and performance-limiting phenomena under realistic cell operating conditions.

Novel Lithium/Polymer-Electrolyte/Sulfur Cells

An electrochemical cell based on the lithium/sulfur couple is attractive as an electric vehicle (EV) power source because of its very high theoretical specific energy (2600 Wh/kg). A primary obstacle in producing a functional Li/S cell is the poor conductivity of sulfur. This difficulty led other researchers to utilize sulfur compounds instead of elemental sulfur, a choice which results in significantly lower theoretical specific energies. We are developing ambient-temperature solid-state Li/S cells using solid polymer electrolytes. The use of a solid polymer electrolyte which is ionically conductive below the melting point of sulfur alleviates some problems encountered by researchers studying high-temperature lithium-sulfur cells (*e.g.*, Li/FeS_2 cells). It also mitigates problems associated with the use of solid lithium metal in liquid electrolytes.

Sulfur electrodes were initially prepared from suspensions of elemental sulfur powder, carbon (graphite), polyethylene oxide (PEO), lithium trifluoromethanesulfonate (LiTf), and Brij 35 surfactant in acetonitrile. These suspensions were cast onto Teflon-coated plates to produce 100-200 μm thick films. Galvanostatic cycling of cells fabricated from these electrodes and PEO-LiTf electrolyte films showed good charge-discharge behavior at low currents (~10 mA/cm²), but resulted in poor utilization of the active material (of order 1-2%). Scanning electron microscopy (SEM) in conjunction with electron spectroscopy for

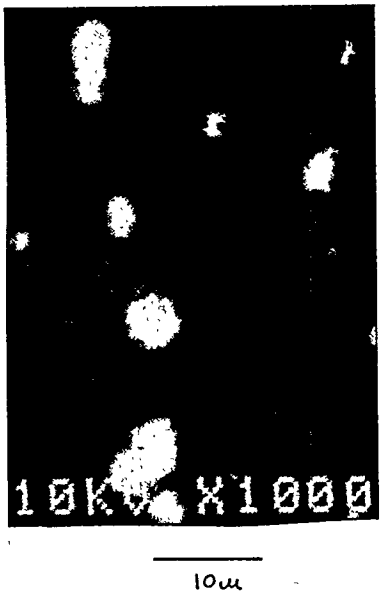

Figure. *Scanning electron micrograph of a small portion of an as-prepared sulfur electrode. Light spots are sulfur-rich islands (as large as 10 μm elsewhere on the electrode).*

*Visiting Scientist

**Materials Sciences Division, LBNL

chemical analysis (ESCA) revealed the presence of 10-μm sulfur islands in the as-prepared sulfur electrodes (Figure). Based on our electrochemical and morphological studies, we have formulated a preliminary phenomenological model of the sulfur electrode. The model postulates the creation of a Li_2S reaction zone which is characterized by slightly higher ionic conductivity but equally poor electronic conductivity, compared to elemental sulfur. In addition, the volume changes that accompany the electrochemical reaction are incorporated into the model, which predicts a loss of available active material. This model makes apparent the need for smaller sulfur particles in the electrode, and various fabrication methods were used to achieve this. The most successful method yet developed involves the dissolution of sulfur in carbon disulfide followed by the addition of this solution to a suspension of the other electrode components. Galvanostatic cycling of some of these electrodes resulted in a utilization of several percent of the active material.

Some unusual results were obtained, however, when these cells were subjected to extended cycling, including much longer charges than discharges and some discharges bearing two distinct plateaus. In addition, many charging plateaus exhibited large, prolonged voltage fluctuations. These results suggest that parasitic reactions may be taking place in the cells or that lithium dendrites may be present. Our data indicate the need to develop spectroscopic methods to analyze the electrodes during and after cycling, and the necessity to refine fabrication protocols to minimize contamination with impurities from the environment. These efforts are now being undertaken. In addition, we are trying to further reduce the size of the sulfur particles in the electrodes, and we are using SEM/ESCA to characterize the electrodes and preparation techniques.

High-Performance Direct-Methanol Fuel Cells

Fuel cells are energy conversion devices that offer the promise of higher efficiencies and greatly reduced emissions, compared to internal combustion engines. Consequently, an application of major interest for these devices is the electric vehicle (EV). However, present-day fuel cells typically operate on H_2, so either a H_2-storage device or a fuel reformer must be carried onboard the vehicle. Each of these H_2-delivery options results in a heavy, bulky, and costly power plant. Therefore there exists a strong need for a fuel cell that can electrochemically oxidize liquid fuels, and successful development of a direct-methanol fuel cell (DMFC) would represent a major advance.

For vehicle applications, only the polymer and alkaline electrolyte fuel cells are considered to be practical because of their low operating temperatures, *i.e.*, they are capable of rapid start-up because they operate below 150°C. The polymer electrolyte fuel cell is an attractive candidate for EV applications, however permeation of CH_3OH through the electrolyte significantly degrades its fuel efficiency and performance. The formation of undesirable reaction products and cathode deactivation also reduce the overall performance of fuel cells with acidic electrolytes. The desired reaction products from the electrochemical oxidation of CH_3OH are H_2O and CO_2. In alkaline electrolytes, carbonation reactions and the formation of carbonate salts have prevented their use in fuel cells that utilize CH_3OH directly. However, buffered electrolytes such as aqueous Cs_2CO_3 reject CO_2 and have shown considerable promise as an electrolyte for the direct oxidation of CH_3OH. Our recent results demonstrated that the direct electrochemical oxidation of CH_3OH on supported Pt/Ru alloy electrocatalyst occurs with a polarization comparable to Pt supported on carbon, but at a lower temperature.

The major goal of this research project is to demonstrate that a Cs_2CO_3 electrolyte fuel cell, utilizing a Pt/Ru anode catalyst for the electrooxidation of CH_3OH, is an efficient and reliable system that produces only H_2O and CO_2 as reaction products. A model fuel cell was designed and fabricated to accommodate 20-cm² electrodes. The electrodes have a bi-layered structure, consisting of a semi-hydrophilic reaction layer which is hot-pressed onto a hydrophobic gas diffusion layer. Electrodes of various catalyst loadings (0.3 to 1.0 mg/cm²) and polytetrafluoroethylene content (15 to 40 wt %) have been prepared and tested in half-cell and full-cell configurations, utilizing both H_2SO_4 and Cs_2CO_3 as electrolytes with H_2 and CH_3OH feeds. Thus far, the full-cell performance has been lower than expected, because of problems with the design of the complete cell. We plan to improve DMFC performance by optimizing the overall design and varying the composition of the electrodes and the electrolyte. Alternative separator materials may also be utilized in future experiments. Analyses of the exit gases will be performed to determine if CH_3OH oxidizes completely to benign reaction products. Engineering design studies of an optimized system will be initiated to assess its suitability for EVs and other applications.

Poisoning of Fuel-Cell Electrocatalyst Surfaces: NMR Spectroscopic Studies

Platinum is the most active single-component catalyst for methanol electrooxidation in DMFCs, however poisoning reactions on the surface in acidic electrolytes render the anode ineffective under target operating conditions. As an approach to designing better catalysts for this system, a number of *in situ, ex situ* and on-line techniques have been utilized to obtain information on the nature of the poisoning intermediate(s). While significant advances have been made, no current *in situ* technique can yield detailed quantitative information on practical (*i.e.* supported, dispersed) electrocatalysts. Nuclear magnetic resonance (NMR) spectroscopy is a quantitative, non-destructive, bulk method of probing the chemical environment of a specific nucleus. During the last two decades the technique has been used successfully in the field of gas-phase catalysis as a tool for identifying and characterizing chemisorbed species on practical catalysts. Our research seeks to extend the application of NMR spectroscopy to studies of surface poisoning of carbon-supported platinum and platinum-alloy DMFC anodes in operating electrochemical cells.

We have constructed a glass three-electrode electrochemical cell for use in a narrow-bore (5 cm) spectrometer operating at a proton frequency of 270 MHz. The working electrode material is commercially prepared 20% Pt/Vulcan XC-72 supported on thin carbon cloth. This cloth is rolled tightly to form a cylindrical porous plug, filling the volume of the NMR coil with an active catalyst surface area on the order of 3 m². The electromagnetic coupling of the conductive electrode material with the coil presents a special problem for these experiments. To minimize this effect, a porous separator is wound with the cloth to electronically insulate adjacent layers of the plug.

We have carried out preliminary studies of the model system of CO adsorbed on Pt. Lending justification to this choice are results of *in situ* IR studies of smooth

Pt electrodes which suggested CO as the main poisoning adsorbate in the CH_3OH electrooxidation reaction. We used a circulation system for adsorption of ^{13}C-enriched CO from saturated aqueous H_2SO_4. As an indirect monitor we used voltammetry to observe the displacement of adsorbed H_2 from the Pt surface by the irreversibly adsorbed CO. To date we have detected the ^{13}C NMR signal arising from ^{13}CO adsorbed on the electrodes described above under open-circuit conditions. We are optimizing the signal-acquisition process to establish the feasibility of NMR to provide *in situ* information on adsorption at the electrode-electrolyte interface. We will then have a firm base for extending our studies to the CH_3OH electrooxidation reaction, *in-situ* potential control, and bimetallic electrocatalyst surfaces.

Anion Adsorption at Electrocatalyst Surfaces: Probe Beam Deflection Study

The rate and extent of anion adsorption on electrocatalyst surfaces can have a major effect on the electrochemical kinetics of important fuel cell reactions such as hydrogen oxidation, methanol oxidation and oxygen reduction. Anion adsorption isotherms are generally difficult to measure, and little reliable data have been reported in the literature. The purpose of this work is to use the *in situ* Probe Beam Deflection (PBD) technique to study the rate and extent of anion adsorption at polycrystalline Pt electrode surfaces as a function of electrode potential. We have carried out a series of PBD experiments to detect the proton and anion fluxes that accompany the oxidation and reduction processes that proceed on Pt electrode surfaces in 0.1 M solutions of H_3PO_4, H_2SO_4 and $HClO_4$. The measured beam-deflection signals exhibited a strong dependence on electrode potential and anion identity. We found that in all three electrolytes the onset of anion adsorption began at ~200 mV (*vs.* the dynamic hydrogen reference electrode), *i.e.*, within the potential range wherein adsorbed H_2 is oxidized. We also confirmed that the presence of PO_4^{3-} anions shifts the Pt oxidation reaction toward more positive potentials.

References

Adler TC, McLarnon FR, Cairns EJ. Rechargeable Zinc cell with alkaline electrolyte which inhibits shape change in zinc electrode. United States Patent #5,453,336 (1995); continuation-in-part of United States Patent No. 5,302,475.

Adler TC, Plivelich RF, McLarnon FR, Cairns EJ. Zinc electrodes. *Proc. Symp. on the Science of Advanced Batteries* 1995. D.A. Scherson, ed., pp. 100-106, Case Western Reserve University, Cleveland, OH.

Brisard GM, Rudnicki JD, McLarnon FR, Cairns EJ. Application of probe beam deflection to study the electrooxidation of copper in alkaline media. *Electrochim. Acta* 1995; 40:859.

Deng Z, Spear JD, Rudnicki JD, McLarnon FR, Cairns EJ. Infrared-photothermal deflection spectroscopy: a new probe for the investigation of electrochemical interfaces. Paper no. 669 presented at the 187th Meeting of the Electrochemical Society, Reno, NV, May 1995.

Plivelich RF, McLarnon FR, Cairns EJ. Degradation mechanisms of nickel oxide electrodes in zinc/nickel oxide cells with low-zinc-solubility electrolytes. *J. Appl. Electrochem.* 1995; 25:433.

Rauhe BR Jr, McLarnon FR, Cairns EJ. Direct anodic oxidation of methanol on supported platinum/ ruthenium catalyst in aqueous cesium carbonate. *J. Electrochem. Soc.* 1995; 142: 1073.

Ridgway PL, McLarnon FR, Cairns EJ. Sodium/phosphorous-sulfur cells. part I - cell performance. *J. Electrochem. Soc.* 1996; 143: 406.

Ridgway PL, McLarnon FR, Cairns EJ. Sodium/phosphorous-sulfur cells. part II - phase equilibria. *J. Electrochem. Soc.* 1995; 143: 412.

Striebel KA, McLarnon FR, Cairns EJ. Steady-state model for an oxygen fuel cell electrode with an aqueous carbonate electrolyte. *Ind. & Engin. Chem. Res.* 1995; 34: 3632.

Taucher W, Adler TC, McLarnon FR, Cairns EJ. Development of lightweight nickel electrodes for zinc/ nickel oxide cells. accepted for publication in *J. Power Sources*, 1996.

Electrode Surface Layers

F.R. McLarnon, R.H. Muller, L. DeSouza**, F.-P. Kong, and R. Kostecki*

We are studying the effects of surface modification on the electrochemical behavior of electrodes used in rechargeable batteries. We use both low-energy (~3 keV) and high-energy (to >100 keV) ion beams to implant dopants into the surfaces of electrodes. Advanced spectroscopic ellipsometry, Raman spectroscopy and traditional electrochemical characterization methods are used to study the structure, composition and evolution of surface layers on these electrodes. The primary objective of this research is to identify film properties that improve the rechargeability, cycle-life performance, specific power, specific energy, and stability of electrochemical cells.

*Materials Sciences Division, LBNL
**Visiting scientist

Raman Spectroscopic Study of Nickel Electrodes

Oxidized nickel [believed to be mostly NiOOH in the charged state and mostly $Ni(OH)_2$ in the discharged state] is the electrochemically active component of the positive electrode in several rechargeable alkaline batteries presently under consideration for use in electric vehicles. There is a strong incentive to better understand the operation of this important electrode and to improve its performance and efficiency. While much is known about the electrochemical properties of the NiOOH electrode, and rechargeable alkaline batteries are in widespread use, the electrode formation process, the kinetics and mechanism of its redox reactions, and the controlling charge/mass transport processes are still not completely understood. Improvements in the NiOOH electrode specific capacity, coulombic efficiency, charge retention and cycle life will lead to enhanced battery performance. We are using Raman spectroscopy, surface-enhanced Raman spectroscopy (SERS) and traditional electrochemical characterization methods to study changes in the electrode phase composition and structural transformations that accompany charge transfer.

The phase transitions which occur in thin $NiOOH/Ni(OH)_2$ films as a result of multiple charge-discharge cycles usually reduce the electrode specific capacity. Freshly precipitated α-$Ni(OH)_2$ is highly disordered and delivers a high specific capacity when oxidized to g-NiOOH, often reaching the $Ni^{+3.7}$ oxidation state. However, the conventional α-

$Ni(OH)_2$ tends to transform irreversibly into the isostructural β-$Ni(OH)_2$ form, which yields a lower average valence state upon oxidation to the β-NiOOH. *In situ* Raman spectra of the charged mass have been successfully recorded and are consistent with previously published data. Numerical deconvolution procedures were applied to the recorded spectra and revealed unique structural information that is not easily obtainable *via* other structural analysis methods. Careful analysis of vibration band parameters allowed us to monitor structural transitions in the charged (oxidized) film which accompanied the electrode capacity loss associated with long-term cycling.

SERS spectra of precursor cathodically deposited a-phases showed that they differ in structure from chemically prepared α-$Ni(OH)_2$. The deconvoluted SERS spectra (Figure) demonstrated that these precursor phases consist of a non-close-packed structure of the α-$Ni(OH)_2$ phase, however the presence of β-like structures was also detected. The presence of such a second phase in the freshly precipitated $Ni(OH)_2$ electrode has not been previously detected using other methods. This result illustrates the ability of Raman spectroscopy to distinguish between different interlayer NiO_2 stacking arrangements.

In situ SERS spectra of the discharged (reduced) film measured during long-term cycling experiments did not resemble the spectra of any known single $Ni(OH)_2$ phase. We deconvoluted these spectra to quantitatively analyze the interconversion between α and β phases. The deconvoluted spectra were characteristic of neither true β-phase material nor the pure α-phase form of the $Ni(OH)_2$. Aging and/or long term charge-discharge cycling processes result in the formation of disordered β-phase materials from the precursor α-like phase. Interestingly, long-term cycling leads to the formation of still another unknown phase which could possibly contribute to electrode capacity loss. We estimate that the charge efficiency of the nickel electrode drops to ~50% of its initial value at the end of the long-term cycling experiments.

The beneficial effect of small additions of certain metals to the NiOOH electrode has been known for a long time. In particular, the addition of 5-10 wt% of Co improves the reversibility of the NiOOH/$Ni(OH)_2$ redox reaction and slows aging processes. We have confirmed that the co-precipitation of Co ions into $Ni(OH)_2$ films reduces the drop in charge efficiency to ~25% after long-term cycling. Examination of the Raman spectra of oxidized active mass showed that Co additions stabilize a structure that is γ-like, characterized by a high average Ni valence state, and exhibits a minimal structural change upon cycling. Incorporation of cobalt ions into the film appears to involve formation of a new phase in the discharged active mass, suggesting that Co doping occurs by substitution of Ni sites.

Experiments to further characterize structural effect of Co incorporation on the electrochemical properties of the NiOOH electrode will continue. To confirm our SERS results, Raman spectroscopy experiments will be attempted using modified, highly absorbing nickel electrodes. Nickel electrodes with overlayers of photosensitive TiO_2 will be investigated as a means to promote the formation of Ni^{4+} compounds.

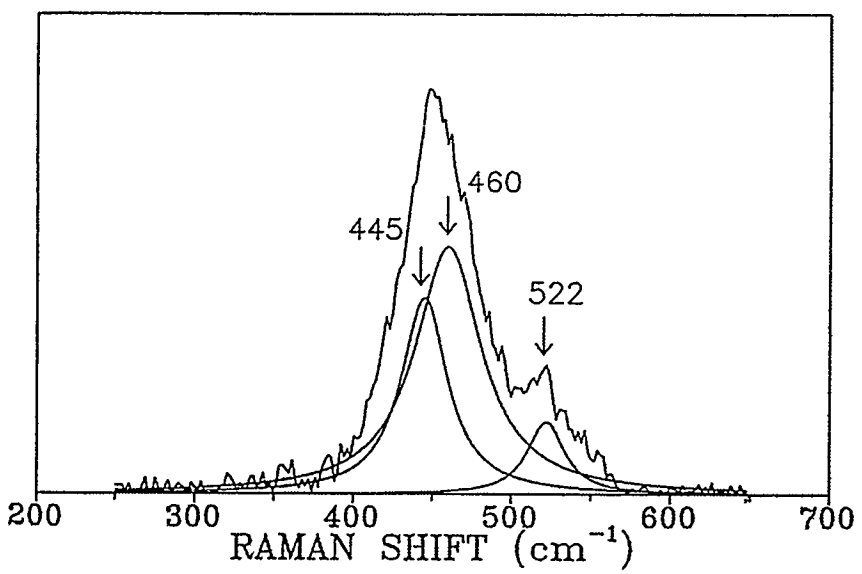

Figure. *In situ surface-enhanced Raman spectrum of cathodic $Ni(OH)_2$ on Ni deconvoluted into three components: β-$Ni(OH)_2$ at 445 cm^{-1}, α-$Ni(OH)_2$ at 460 cm^{-1}, and an unknown phase which correlates with electrode failure at 522 cm^{-1}.*

Characterization of Nickel Electrodes by Spectroscopic Ellipsometry

We are using *in situ* spectroscopic ellipsometry and cyclic voltammetry to study the properties of anodic oxide films formed on polycrystalline Ni electrodes. Preliminary studies were carried out in 1 M NaOH electrolytes under potentiodynamic conditions at 10 mV/s over the range -0.9V to 0.0V *vs.* Hg/HgO. First, polished Ni was exposed to air and ellipsometric measurements were made. Deconvolution of the ellipsometric data using the effective medium approximation technique indicated the presence of a 2-nm-thick film of NiO, as well as significant roughness at the Ni/NiO and NiO/air interfaces. Measurements were then carried out at -0.4 V and 0.0 V, which are associated with the initial formation and growth of $Ni(OH)_2$, respectively. Measurements were made when the Ni electrode potential first reached 0.0 V and following a 2-h hold at this potential.

Deconvolution of the ellipsometric data recorded at -0.4 V indicated that the anodic layer is ~1.4 nm thick (including the roughness of the metal and oxide) at this potential, and can be described as a mixture of 50 vol% NiO plus 50 vol% $Ni(OH)_2$. When the electrode potential first reached 0.0V the anodic layer grew to 2.4 nm thick and its composition changed to 30 vol% $Ni(OH)_2$ with the balance NiO. After holding at 0.0 V for 2h the anodic layer grew to ~15.6 nm and contained only $Ni(OH)_2$. It is interesting to note that the electrode potential never reached -0.9 V, where one might expect the reduction of the air-formed NiO film.

Surface Modification of Lithium Electrodes

Rechargeable Li batteries are attractive because of their high specific energy, however they exhibit short lifetimes and safety problems, in part because of the poor stability of the surface layers that form spontaneously on metallic Li

electrodes in liquid organic electrolytes. The high ionic conductivity and chemical stability of Li_3N suggest its use as a protective surface layer, but prior attempts to form a compact, nonporous Li_3N surface layer have not succeeded because of the large difference between the molar volumes of Li and Li_3N. We have now used the LBNL low-energy ion implantation and plasma-assisted deposition facility to form compact and homogeneous nitrided lithium surface layers. We used ESCA to measure 3-6 atomic percent nitrogen at the nitrided electrode surface, and SEM images of as-grown nitrided Li surfaces showed island structures with a characteristic sizes of ~20 μm, and no macroscopic cracks or other inhomogeneities were detected.

We fabricated Li/propylene-carbonate (PC)/stainless-steel and Li/PC/MnO_2 cells with and without protective Li_3N layers on the Li electrodes. Cyclic voltammetry tests showed that cells with protective Li_3N layers can be operated in a stable manner up to ~4.4V, which is comparable to the behavior of Li-ion cells. We also prepared 3-electrode cells and measured the cell capacity as a function of current density over the range 0.2 to 2.0 mA/cm². The polarization characteristics of the nitrided lithium electrode were quite different from those observed in cells with untreated lithium electrodes. Features associated with unwanted Li dendrite growth that accompany the repeated charging and discharging of Li/PC cells are absent in the cells with protective Li_3N layers. Cycle-life performance tests are being carried out at 0.5 mA/cm² between discharge/charge potential limits of 3.35 and 4.35 V, respectively. After the first 40 cycles, the capacity of a cell with a nitrided lithium electrode decreased by ~30%, whereas a similar cell with a pure Li electrode decreased by ~40% under the same cycling conditions. These preliminary tests with unoptimized electrodes clearly demonstrate the beneficial effects of using protective Li_3N layers in rechargeable cells with liquid organic electrolytes. We plan to establish a model to describe interfacial behavior in these cells, using spectroscopic ellipsometry and other analytic techniques to characterize their properties under typical cell operating conditions.

References

Anders S, Anders A, Brown I, Kong F, McLarnon F. Surface modification of nickel battery electrodes by cobalt plasma immersion ion implantation and deposition. (accepted for publication in *Surface & Coatings Technology*, 1996)

Anders S, Anders A, Brown I, McLarnon F, Kong F. Synthesis of metal suboxide films for battery applications by cathodic arc deposition. Invention Disclosure No. IB-1106 (1995).

McLarnon F, Kong F, Anders S, Anders A, Brown I. Use of plasma processing to stabilize the interface between a lithium electrode and a polymer electrolyte. Invention Disclosure No. IB-1102 (1995).

Wang K, Ross PN Jr, Kong F, McLarnon F. The reaction of clean Li surfaces with small molecules in UHV: I. dioxygen. *J. Electrochem. Soc.* 1995; 143: 422.

Analysis and Simulation of Electrochemical Systems

J. Newman, R. Darling, C. M. Doyle, C.-P. Lau, J. Meyers, B. Paxton, B. Pillay, and K. Podolske

This program involves fundamental investigations of the transport and interfacial phenomena important in electrochemical systems. Results of this work are used to analyze experimental data, to identify important system parameters, and to aid in the design and scale-up of electrochemical systems. The approach taken is to develop a detailed mathematical model of the device using the principles of transport phenomena, reaction kinetics, and thermodynamics. The mathematical models are developed to be as general as possible without unnecessary mathematical or physical approximations. The resulting sets of coupled equations are then solved numerically, which permits the complex interactions between phenomena to be treated. Experimental work may then be used to confirm and refine the mathematical models and to determine the physical parameters necessary for a complete, quantitative understanding of the system.

Lithium-based rechargeable batteries have been explored in detail using mathematical modeling. The first-generation model has been expanded to treat film formation on the electrode surfaces and temperature rise during nonisothermal discharge. The model is also able to simulate charge/discharge schemes more complicated than just galvanostatic ones, for example, potentiostatic taper charges, power pulses, and extended cycling. The specific lithium systems that are being explored include a lithium foil cell consisting of a polymer electrolyte and a manganese oxide spinel positive electrode. This system has been studied in detail in order to determine the tradeoffs in system performance that occur as the transport properties of the polymer electrolyte, especially ionic conductivity and lithium ion transference number, are varied.

The modeling work also emphasized the importance of accurate transport property data to the design process. The necessary transport properties are rarely available for even the most common lithium salt and solvent combinations. This problem is even worse for solid-polymer electrolytes where the methodology to measure the lithium ion transference number without the assumption of an ideal solution does not exist. Motivated by this situation, a novel method to measure the transference number has been developed. This method is not only easy to carry out, but also involves no assumption about the ideality of the solution. In order to demonstrate the generality and validity of this method, it is being applied to the measurement of the potassium ion transference number in aqueous potassium chloride solution of several different concentrations. The experimentally determined transference numbers are found to be within 1% agreement with the literature values. This method has also been used to measure the sodium ion transference number in a concentrated solid polymer electrolyte solution.

Experiments have shown that an electrochemical cell having a composite positive electrode containing lithium manganese oxide and carbon black, a lithium perchlorate in propylene carbonate electrolyte, and a lithium foil negative electrode exhibits behavior indicative of a side reaction at the positive electrode. Such a cell will cycle with a coulombic efficiency of less than 100% and will completely self-discharge if left at open cir-

cuit for a long time. This behavior is expected to affect the performance and safety of lithium batteries. A model of this system is being developed which will consider the main insertion reaction in the cathode as well as a side reaction occurring predominantly on the conductive filler. This model will be used to guide experiments into the nature and significance of the side reaction.

The variable diffusivity in intercalation material is also being studied. A theoretical approach for estimating a "best" constant diffusion coefficient to use in an electrode model is developed for the case where experimental data on the diffusion coefficient as a function of the state of charge for an intercalation material are available. This method uses a model of diffusion in a single particle as its basis. From examining the surface concentration *vs.* average concentration curve for diffusion in a single particle, we can determine a diffusion coefficient that is a function of the dimensionless flux rate of material into the particle. This diffusion coefficient function can then be used in a model of a porous electrode.

The solid state diffusion coefficient of protons (H^+) in nickel oxide insertion compounds has been experimentally determined using an intermittent galvanostatic method. The diffusion coefficient of protons was found to range between 8×10^{-14} to 8×10^{-13} cm^2/s for ~1-μm-thick sol-gel deposited nickel oxide. The range of diffusion coefficients obtained demonstrates the dependence of the diffusion coefficient on the state of charge of the nickel oxide. The film preparation, characterization, and diffusion coefficient measurement methods used in this work are generally applicable to most insertion materials. The accurate determination of proton diffusion coefficients is important for the optimization and design of devices which employ insertion materials. The dependence of the diffusion coefficient on temperature, electrolyte concentration, and film thickness are under investigation.

A fairly comprehensive model of electrochemical capacitors has been developed. The model is based on pseudo-homogeneous porous-electrode theory. Concentrated-solution theory is used to predict the mass transfer. The capacity to treat multiple faradaic reactions, including side reactions and those leading to faradaic pseudocapacitance, is incorporated. Simulations allow us to identify the physical processes that govern the behavior of these systems, as well as to investigate the dependence of performance on various design parameters. The model is being used to test the potential of different systems; the specific systems being modeled include carbon electrodes in aqueous sulfuric acid, ruthenium oxide electrodes in aqueous sulfuric acid, and carbon electrodes in propylene carbonate with a suitable salt. The influence of side reactions on the behavior of the carbon electrodes in aqueous sulfuric acid system has been shown to be fairly important. With consideration of side reactions, the model predicts some of the anomalous behavior seen in experiments on similar devices. The model is fairly general, and can be extended to treat other systems and effects.

A mathematical model of the discharge behavior of the nickel oxide/KOH/$LaNi_5$ battery system has been developed. The model shows great sensitivity to the kinetic parameters of the nickel oxide active material. The electrode thickness and porosity of the battery system are optimized in terms of the specific energy and power of the system.

References

Newman J. Optimization of porosity and thickness of a battery electrode by means of a reaction-zone model. *J. Electrochem. Soc.* 1995; 142: 97-101.

Doyle M, Reimers J, Newman J. A quick method of measuring the capacity versus discharge rate for a dual lithium ion insertion cell undergoing cycling. *J. Power Sources* 1995; 52: 211-216.

Wang MH, Newman J. The electrical conductivity of sodium polysulfide melts. *J. Electrochem. Soc.* 1995; 142: 761-764.

Tiedemann W, Newman J. Temperature rise in a battery module with constant heat generation. *J. Electrochem. Soc.* 1995; 142: 1054-1057.

Fuller TF, Newman J. Metal hydride electrode. In: R.E. White, J.O'M. Bockris, and B.E. Conway, eds. *Modern Aspects of Electrochemistry.* 1995; 27: 359-383.

Doyle M, Fuller TF, Newman J. Theoretical modeling of battery systems. In: D.A. Scherson, ed. *Proceedings of the Symposium on the Science of Advanced Batteries.* 1995; 152-163.

Battaglia V, Newman J. Modeling of a growing oxide film: the iron/iron oxide system. *J. Electrochem. Soc.* 1995; 142: 1323-1430.

Trainham JA III, Law CG Jr, Keating KB, Eames DJ, Newman J. Electrochemical conversion of anhydrous hydrogen halide to halogen gas using a cation-transporting membrane. United States Patent No. 5,411,641. May 2, 1995.

Doyle M, Newman J. Modeling the performance of a rechargeable lithium-based cells: design correlations for limiting cases. *J. Power Sources* 1995: 54: 46-51.

Ma YP, Doyle M, Fuller TF, Doeff MM, De Jonghe LC, Newman J. The measurement of a complete set of transport properties for a concentrated solid polymer electrolyte solution. *J. Electrochem. Soc.* 1995; 142: 1859-1868.

Pals CR, Newman J. Thermal modeling of the lithium/polymer battery. I. Discharge behavior of a single cell. *J. Electrochem. Soc.* 1995; 142: 3274-3281.

Pals CR, Newman J. Thermal modeling of the lithium/polymer battery. II. Temperature profiles in a cell stack. *J. Electrochem. Soc.* 1995;142: 3274-3281.

Rush B, Newman J. Periodic behavior in the iron/sulfuric acid system. *J. Electrochem. Soc.* 1995; 142: 3770-3779.

Doyle M, Newman J. The use of mathematical modeling in the design of lithium/polymer battery systems. *Electrochim. Acta* 1995; 40: 2191-2196.

Eames DJ, Newman J. Electrochemical conversion of anhydrous HCl to Cl_2 using a solid-polymer-electrolysis cell. *J. Electrochem. Soc.* 1995; 142: 3619-3625.

Newman J. Thermoelectric effects in electrochemical systems. *Ind. Engr. Chem. Research* 1995; 34: 3208-3216.

Doyle M, Newman J. Analysis of transference number measurements based on the potentiostatic polarization of solid polymer electrolytes. *J. Electrochem. Soc.* 1995; 142: 3465-3468.

Fuller TF, Newman J. Diffusion. *Encyclopedia of Chemistry* (Macmillan Publishing Co.), submitted October, 1992.

Trainham JA III, Law CG Jr, Keating KB, Eames DJ, Newman J. Anode useful for electrochemical conversion of anhydrous hydrogen halide to halogen gas. United States Patent application, May 20, 1994.

Doyle M, Newman J, Gozdz AS, Schmutz CN, Tarascon JM. Comparison of modeling predictions with experimental data from plastic lithium ion cells. July, 1995. Lawrence Berkeley National Laboratory Report No. LBL-36977. (also submitted to *J. Electrochem. Soc.*)

Doyle M, Newman J. Analysis of capacity-rate behavior using simplified models for the discharge process of lithium batteries. April 1995. Lawrence Berkeley National Laboratory Report No. LBL-36244. (submitted to *J. Appl. Electrochem.*)

Newman J. Electrostatic systems and electrochemical systems. Lawrence Berkeley National Laboratory Report No. LBL-37457. Presented at the 187th Meeting of the Electrochemical Society, Reno, NV, May 1995, and published in the *Proceedings*.

Paxton B, Newman J. Variable diffusivity in intercalation materials—a theoretical approach. August 1995. Lawrence Berkeley Laboratory Report No. LBL-37550. (submitted to *J. Electrochem. Soc.*)

Paxton B, Newman J. Modeling of nickel/metal hydride batteries. I. Model of the nickel oxide/KOH/$LaNi_5$ system. September, 1995. Lawrence Berkeley National Laboratory Report No. LBL-37745. (submitted to J. *Electrochem. Soc.*)

Paxton B, Newman J. *Modeling of Nickel/Metal Hydride Natteries. II. Solid-State Diffusion Limitations in the Nickel Oxide Electrode.* Lawrence Berkeley National Laboratory Report No. LBL-37746, September 1995. (also submitted to *J. Electrochem. Soc.*)

Pillay B, Newman J. The Influence of Side Reactions on the Performance of Electrochemical Double-Layer Capacitors. Lawrence Berkeley National Laboratory Report No. LBL-37543, September 1995. (also submitted to *J. Electrochem. Soc.*)

Heat Transport and Thermal Management in Advanced Batteries

J.W. Evans and Y. Chen

Thermal management is crucial to the safe operation of, and the achievement of optimal/normal performance of, electric vehicle batteries. The objective of this project is to examine , by mathematical modeling and experimental measurement, battery thermal behaviour and suitable thermal management systems, and to evaluate battery energy efficiency and the possibility of the occurrence of thermal runaway due to battery abuse. A similar approach will also be applied to solid oxide fuel cells.

A three-dimensional model is developed to simulate and compare heat generation and transport within a lithium/polymer-electrolyte battery under galvanostatic discharges and the SFUDS dynamic power profile. Emphasis has been placed on the maintenance of the operational temperature and temperature uniformity within a battery by designing a suitable thermal management system. The results indicate that, on the one hand, because of the low effective thermal conductivity across a laminated cell stack, steep temperature distributions may be caused if cooling channels or electric heaters are placed at the two ends of a cell stack. On the other hand, the relatively large average thermal conductivity along the width and height directions allows more efficient heat removal or addition, and thus facilitates the maintenance of uniform operating temperature. The thermal model has been applied to study the effectiveness of different arrangements of cooling channels and electric heaters and to select suitable heating intensities and insulating materials.

The calculations of the temperature rise in the Sandia conceptual battery designs for Ford Van and GM Impact, during constant current discharges and a DST/Fast Charge/DST/Full Charge cycle, have been conducted, with the three-dimensional thermal model. Also, a comparison of heat generation rates within a lithium/polymer-electrolyte battery during the DST and SFUDS dynamic power profile was carried out.

The main concern with the thermal behaviour of the room-temperature lithium-ion batteries is the possible significant temperature increase which may cause thermal runaway. The modeling results indicate that, during normal battery operation, battery temperatures are unlikely to reach the onset temperature for thermal runaway, although heat may not be dissipated out of a large cell stack during high-rate discharge (*e.g.*, during the short time period of a high-pulse power extraction from a battery). However, if a battery is continuously cycled under high-rate charge and discharge, significant heat accumulation within a battery may be caused. The analysis of heat transfer in the existence of highly localized heat sources due to battery abuse (*e.g.*, short circuit) indicates that localized heating may raise battery temperature, within one minute, to the thermal runaway onset temperature, above which battery temperature may keep increasing rapidly due to exothermic side reactions triggered at high temperature.

To provide answers to the concern as to how quickly the temperature of solid oxide fuel cells (SOFCs) for transportation application will drop, a thermal analysis of the cool-down time of a SOFC stack during vehicle idle or standby has been carried out. Because a large amount of thermal energy is stored in high-temperature SOFC stacks, it is important to select suitable thermal insulations to reduce heat loss. The results indicate that a high-performance, vacuum-multifoil thermal insulation can be applied to significantly reduce heat loss and to maintain temperature uniformity across a cell stack. Consequently, the cooldown time from 1000 to 800°C is extended from 2 h (with a 5-cm thick conventional material) to about 31 h (with a 1-cm-thick high-performance material).

Systematic investigation of the thermal conductivity of cell components, and the effective properties of cell stacks, of lithium/polymer-electrolyte batteries is underway. The total energy efficiency of the lithium/polymer-electrolyte battery will be evaluated by including the energy consumption for heating the battery before vehicle startup or during vehicle standby, and by taking into account of the statistical data of the commute length (journey-to-work) of the general public. The thermal models will also be extended to examine the thermal behaviour of nickel/metal-hydride batteries.

References

Chen Y, Evans JW. Thermal management of lithium/polymer-electrolyte batteries for electric vehicle application. In: S. Megahed, B.M. Barnett, and L. Xie, eds. *Rechargeable Lithium and Lithium-Ion Batteries,* PV 94-28. Pennington, NJ: The Electrochemical Society, Inc. 1994; 73.

Chen Y, Evans JW. *Application of LBL Thermal Model to Calculation of Temperature Rise in C/polymer Electrolyte/*

$LiMn_2O_4$ Batteries of Sandia Conceptual Designs for Ford Van and GM Impact, and to Examination of Thermal characteristics of a $Li/P(EO)_8LiClO_4/TiS_2$ cell during USABC Dynamic Stress Test (DST) power profile. LBL-37686, July 1995.

Chen Y, Evans JW. Thermal analysis of lithium-ion batteries. (submitted to *J. Electrochem. Soc.*, November 1995)

Chen Y, Evans JW. Cool-down time of solid oxide fuel cells intended for transportation application. (accepted for publication in *J. Power Sources*, September 1995)

Carbon Electrochemistry/Surface Morphology of Metals in Electrodeposition

*K. Kinoshita, X. Song, C.W. Tobias, G. Matzen, R. Stover, J. Newman, and M. Denn**

This project involves investigations of *i)* the role of physicochemical properties of carbonaceous materials on their ability to reversibly intercalate Li, *ii)* the role of electric field and solution-side mass transport in the electrocrystallization of metals: mechanisms of initiation, growth and propagation of imperfections and development of surface textures; and *iii)* the characterization of the physical processes involved in the evolution of gases at electrodes.

Carbon Electrochemistry

This effort is coordinated with the research conducted at LLNL to evaluate the intercalation of Li in carbonaceous materials for rechargeable Li batteries. Studies of samples obtained from commercial vendors, as well as several that were synthesized in-house, are continuing. In particular, the systematic study of the physical properties of carbonaceous materials by utilizing electron microscopy (facilities at the National Center for Electron Microscopy) and x-ray diffraction analysis is underway. The results to date show that graphite powders, both natural and synthetic, which have d(002) spacing of 0.3354 nm, yield the theoretical capacity for Li intercalation, LiC_6.

A new effort was initiated to understand the mechanism of lithium storage by exploring the use of *in situ* TEM to investigate the microscopic changes that occur during lithium intercalation/de-intercalation of carbonaceous materials. The preliminary design and component fabrication of a hermetically sealed cell for *in situ* TEM studies have been completed. The cell is fabricated by growing thin Si_3N_4 membranes on top of a Si wafer. The backside of the wafer is then etched to form small windows of the electron-transparent membrane which should be about 100-nm thick. Electrode materials are subsequently patterned on the membranes such that the desired electrode/electrolyte interfaces are visible through the window. The cell is completed by "sandwiching" the electrolyte between two membranes and sealing the edges of the cell with a suitable material. Several cells have been fabricated and the structure of the thin Si_3N_4 membranes are being examined by TEM. As a prelude to the *in situ* studies, lithiated carbon samples were prepared *ex situ*, and examined by TEM. Samples of lithium intercalated graphite, which were synthesized by chemical lithiation, were examined by TEM and XRD analysis. The samples, which are dark yellow in color and indicative of a stage-one compound, showed the presence of both LiC_6 and LiC_{12} phases. In the future, lithiated graphite that is formed on a Si_3N_4 membrane will be examined by TEM.

Surface Morphology of Metals in Electrodeposition

The local mass transport distribution around microscale protrusions in an electrolyte flow channel was studied by measuring the local currents for a redox couple (Fe^{3+}/Fe^{2+}) at a segmented electrode. The segmented electrode was designed and fabricated in the Microfabrication Laboratory of EECS on the Berkeley campus and consisted of an array of 22 Pt microelectrodes (50-μm square) positioned around the protrusion (~50 μm height and ~85 μm diameter). With this array of microelectrodes, the following results were obtained. When the bulk fluid flow is laminar, mass transport is impeded in the vicinity of the protrusion, and it is impeded the most in the immediate wake. For example, at Re_p = 0.56 the current density is reduced (relative to the current density which would be measured in the absence of a protrusion) by 25% at a location of 100 μm downstream of the protrusion but by only 15% at 100 μm in front of the protrusion. This effect changes with increasing Reynolds number. At Re_p = 3.4, the current is reduced by 30% downstream and by only 7% upstream at the same microelectrode locations. The influence of protrusions on mass transport is qualitatively similar in turbulent flow for Re_p of up to about 50. At higher Reynolds numbers, mass transport is enhanced by a factor of about 1.5 at 100 μm in front of the protrusion and about 1.5 at 250 μm downstream.

A high-speed laser-illuminated photodetector array and associated data acquisition system has been employed for the study of coalescence between electrolytically generated gas bubbles. The fast phenomena associated with the coalescence and separation from the surface of two electrolytically generated hydrogen bubbles, 50 to 600 μm in diameter, is recorded with a resolution of 10^{-5} seconds. In agreement with theoretical predictions, the coalescence event is completed in less than 10^{-3} sec. The experimental results show that the position of the interface in the coalescence plane (*i.e.*, the saddle point between two bubbles) rapidly accelerates to 200 to 400 cm/s. The initial motion is followed by large amplitude oblate-prolate oscillations at frequencies of 0.4 to 17 kHz which are dampened in 0.3 to 10 ms during bubble coalescence. The oscillation frequency is proportional to the square root of the surface tension, inversely proportional to the bubble radius raised to the 3/2 power, and independent of the electrolyte viscosity. The oscillations decay at a rate proportional to the viscosity and inversely proportional to the square of the radius.

**Materials Sciences Division, LBNL*

Fundamental Characterization of Carbon-Based Materials for Electrochemical Systems

K. Kinoshita and X. Chu

A fundamental research program on the synthesis, characterization and modification of carbon-based materials to improve their properties for use in electrochemical systems is underway that involves studies on: (*i*) oxygen reduction on carbonaceous materials in alkaline electrolyte and (*ii*) electrochemical double layer capacitance of porous carbon electrodes. The results are summarized here.

Oxygen Reduction on Carbonaceous Materials in Alkaline Electrolyte

The freshly cleaved basal plane of highly oriented pyrolysis graphite (HOPG), which possesses an atomically smooth surface with few defects and offers an inactive surface for electrochemical reactions, was used as a prototypical carbon electrode to study the effects of surface modification and treatments on the kinetics of oxygen reduction. This surface was modified in a well-controlled manner to increase the surface density of edge sites by exposure to an oxidizing atmosphere at different temperatures. Gas-phase oxidation was conducted in a tube reactor as previously described by Chu and Schmidt [1]. Graphite electrodes were heated in air at 1.0 atm from 500 to 750°C for various time, and then examined by scanning tunneling microscopy (STM).

The STM studies of the HOPG basal plane after heating at 600°C in air for 10 min. showed that uniform monolayer pits were formed and randomly distributed on the basal plane of graphite. However, when the HOPG sample is heated at higher temperatures, two distinguishing processes are involved in the surface etching process: (a) oxygen reacts with the carbon atoms at the original defect sites such as steps and surface vacancies, and (b) oxygen reacts with the carbon atoms in the basal plane of graphite creating new defect sites, which act as nuclei for the growth of the surface monolayer pits. Comparison of the typical ring and disk current distribution of a freshly cleaved and an oxidized HOPG basal plane (air at 700°C for 30 min.) at different rotation speeds in 0.1 M KOH at room temperature showed that the O_2 reduction current increased significantly following oxidation of the basal plane. This change is attributed to the increase in the density of active surface sites at the etch pits which are formed during oxidation.

Electrochemical Double-Layer Capacitance of Porous Carbon Electrodes

The effort in this study is to investigate the relationship between surface structure/surface groups associated with carbon electrodes and the double-layer capacitance. Active carbon fibers AFC (A-10, Spectrocorp; 10-15 mm, 1000 m^2/g) and low-surface-area carbon fibers were used in this study. Three representative low-surface-area carbon fibers were chosen: 1) rayon carbon fibers from regenerated cellulose (Du Pont); 2) polyacrylonitrile (PAN)-based fiber T-8000 (Toray); and 3) mesophase pitch-based carbon fibers (Amoco).

Because the low-surface-area carbon fibers have a relatively low capacitance, a catalytic process was employed to expose more surface sites or to create specific active sites. The fibers were preloaded with a small fraction of nickel (0.2 to 0.5 at%) on the surface using a nickel acetate solution and then treated in air or H_2 to partially remove the surface of the carbon fiber to expose different sites. This process also introduced a different microstructure and pore distribution of the fiber surface to improve the transport properties. The double-layer capacitance was determined in 1.0 M H_2SO_4 by cyclic voltammetry.

SEM analysis of the surface of a rayon carbon fiber, which is generally smooth, showed no detectable fine structure down to 0.1 mm However, after catalytic etching of the carbon fiber with 0.02% Ni in 5% H_2/He at 500°C for 30 min. it was apparent that many pits were formed on the surface by this treatment. The surface of the carbon fiber after further heating at 600°C in H_2 for 30 min. showed an open and interconnected pore structure. Applying the same treatment to PAN fiber results a similar structure, however, for the mesophase carbon fibers, catalytic etching removes the surface layer.

An electrochemical double-layer capacitance of 240 F/g carbon is obtained with A-10 ACF, which after oxidation in air (400°C for 30 min), the capacitance increased only slightly to 260 F/g. After oxidation in air, the capacitance of the rayon and PAN fibers increased about 60% and the mesophase carbon fibers showed a capacitance increase of about 100%. However, after the catalytic etching, the capacitance of the fibers increased dramatically; the mesophase carbon fibers showed an increase in capacitance of about twenty times while those for the other two fibers only doubled. These difference in the capacitance of carbon fibers after treatment is attributed to the microstructures of the three fibers. For the rayon and the PAN fibers, the catalytic treatments increase the surface area which results in an increased capacitance. However, for the mesophase carbon fiber, a high density of graphite edge sites are exposed which are the key for enhancing the capacitance. Therefore designing fiber structure with high external surface area and radial orientation of the graphitized plane, for example, will enhance the capacitance.

Reference

Chu X, Schmidt L. *Carbon 1991*; 29: 1251; *Surf. Sci.* 1991; 268: 325; *Ind. Eng. Chem. Res.* 1993; 32: 1359.

XAS Studies of Electrode Materials for Lithium Batteries

E.J. Cairns, S.P. Cramer, and C. Horne

We seek to establish how Li intercalation affects the atomic and electronic structure of Li-Mn-O spinels used in Li secondary batteries. We use a variety of XAS and electrochemical techniques with the intent of developing a solid-state reaction mechanism based upon the aforementioned types of structural change. This information will be used to identify beneficial material parameters providing increased capacity, improved cyclability, and/or higher rate capacities.

Manganese dioxide (MnO_2) spinel-based electrodes are the most promising for Li^+-intercalation batteries when considering a combination of specific energy, cost, availability, toxicity, and electrode potential. However, batteries derived from these materials display reaction-rate limitations (which affect the battery specific power) and capacity fading that circumvent their present usefulness and commercial viability.

Upon Li intercalation, the Mn sites in MnO_2-spinel based host materials are reduced from Mn(IV) to Mn(III), and the structure changes to accommodate the Li intercalate at empty tetrahedral or octahedral sites. Therefore, changes in the atomic structure as well as the Mn 3d states occur during the reaction. Previous research on MnO_2-spinel based electrode materials combined electrochemical characterization with structural information obtained from x-ray and/or neutron diffraction studies. Investigators found that, upon discharging, when the average Mn-oxidation state is reduced below 3.5 ($x > 1.0$ in $Li_xMn_2O_4$), a cooperative Jahn-Teller distortion takes place, which lowers the spinel's symmetry from cubic to tetragonal symmetry and expands the unit cell volume by 5-6%. Figure 1 shows the open-circuit voltage as a function of Li content in $Li_xMn_2O_4$ for $0 < x \leq 2.2$. There are two voltage plateaus when the Li^+ content is varied over the full range, the 4 volt plateau for $0 < x < 1$, and the 3 volt plateau for $1 < x < 1.8$. Introduction of dopants and cation vacancies into $LiMn_2O_4$ has yielded improved Li intercalation properties. Dopants were shown to be superior to cation vacancies for improving cell cycling stability. Due to the nature of XRD and neutron diffraction techniques, these studies have provided a long-range atomic structural picture as well as an indirect approach to interpreting electronic structure information.

We use electrochemical characterization techniques to help interpret XAS spectra. The electrochemical techniques are cyclic voltammetry, repetitive galvanostatic cycling, and potential-step voltammetry. The XAS techniques employed to this point can be grouped into three main categories: 1) X-ray Absorption Near Edge Spectroscopy (XANES), 2) Extended X-ray Absorption Fine Structure (EXAFS), and 3) K_b Emission Spectroscopy. K-edge XANES and EXAFS give information on the local atomic structure about the absorbing atom, which can also be used to interpret the electronic configuration of the absorber. The absorbing atom's electronic structure is directly determinable by K_b Emission Spectroscopy and $L_{2,3}$-edge XANES as these techniques detect transitions involving the absorbing element's valence states.

During 1995 we characterized the base material $LiMn_2O_4$. Physical and chemical characterization of this material included atomic absorption, B.E.T. surface area, XRD, and SEM. Electrochemical characterization was carried out in swagelok-type cells within a He glove box and included galvanostatic cycling, cyclic voltammetry, and potential step voltammetry. Additionally, a series of XAS measurements was performed on electrochemically intercalated compositions $Li_xMn_2O_4$, $0 < x \leq 2.2$ (Figure 1). The electrochemical intercalation was performed slowly and the electrodes were allowed to reach open-circuit potentials after the calculated charge was passed to achieve the desired lithiated state, x. The XAS measurements included K-edge XANES & EXAFS, K_b emission, and $L_{2,3}$-edge absorption. Figure 2 (see next page) shows the Mn K-edge XANES data set. Along the 4-V plateau, the spectra all correspond to octahedral symmetry of the oxygen ligands about the Mn. Small distortions of the Mn local environment occur due to Li^+ intercalation and are reflected by the inflection seen in the edge spectra. These observations are consistent with a cubic spinel structure. However, along the 3-V plateau a step develops in the absorption edge, which is indicative of octahedral distortion caused by the Jahn-Teller effect and the resultant tetragonal symmetry of the highly lithiated phase. The Mn K-edge main peak results primarily from $1s \rightarrow 4p$ transitions. As the Jahn-Teller distortion occurs, the oxygen octahedra surrounding the Mn elongate along the z-axis. The larger Mn-O distance along the z-axis splits the degeneracy of the Mn 4p states by lowering the energy of the $4p_z$ orbital relative to the $4p_x$ and $4p_y$ orbitals, giving the observed step in the XANES.

In the coming year, doped spinels will be synthesized, Li intercalated within electrochemical cells, and analyzed by

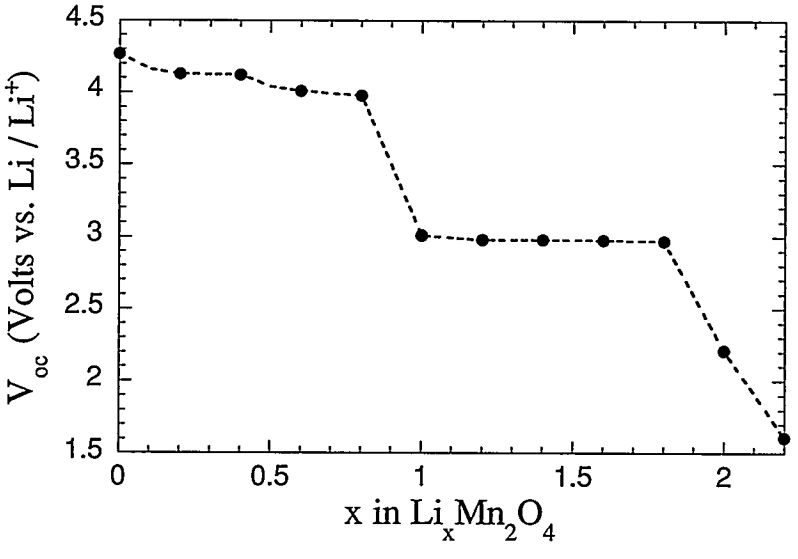

Figure 1. *Open-circuit voltage as a function of lithium content, x, in $Li_xMn_2O_4$.*

the above-described XAS techniques. Atomic and electronic structural changes can then be correlated with electrochemical performance via the techniques described above to identify how the modified spinels behave compared to $LiMn_2O_4$. Based on this information, spinels with alternate dopant concentration or type can be synthesized to obtain optimum cell performance.

We expect to obtain an atomic-level understanding of how the Mn 3d orbitals adapt to Li intercalation in various MnO_2-spinel materials, and to establish relationships between the electrochemical information, the $L_{2,3}$-edge, and K-edge XAS results. This information should allow us to deduce the important compositional and structural properties necessary for the most complete and reversible reactions of lithium with MnO_2-spinel materials and point the way towards synthesizing significantly improved battery materials.

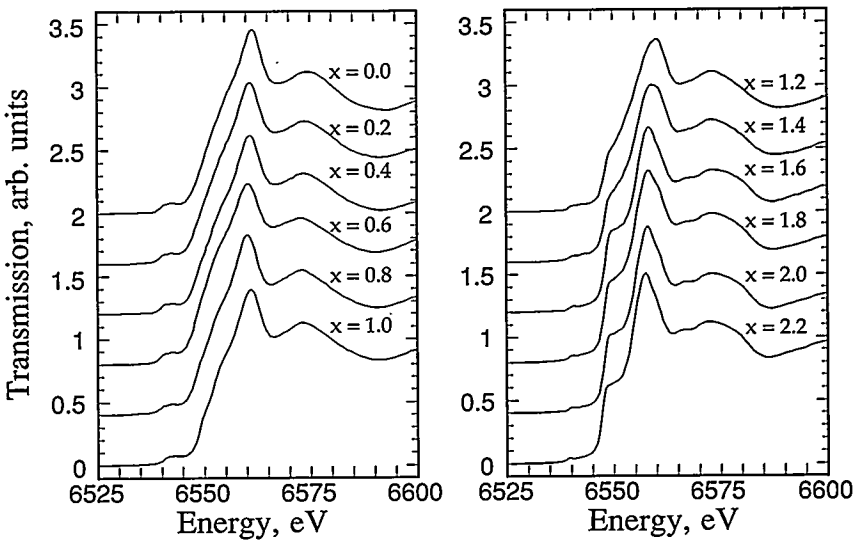

Figure 2. *Mn K-edge XANES of electrochemically intercalated $Li_xMn_2O_4$, $0 < x \leq 2.2$*

Application of Pulsed Laser Deposition to the Study of Rechargeable Battery Materials

K.A. Striebel, C. Deng, S.J. Wen, L. Ma, and E.J. Cairns*

The aim of this project is to study performance-limiting phenomena in complex metal oxides, present in a wide variety of rechargeable batteries, and to suggest practical means for improving their performance and lifetime in secondary consumer batteries. We prepare thin dense films from these oxides on electronically conductive substrates utilizing the pulsed laser deposition technique. This method is superior to other film-formation techniques, such as sputtering and vapor evaporation, based on both speed and simplicity. Films are characterized with x-ray diffraction, x-ray absorbence, XPS, optical and scanning electron microscopy and profilometry. In addition, the groundwork has been laid for characterization of films with Fourier Transform Infrared Spectroscopy (FTIR).

Transmission-mode FTIR spectra were obtained from $Li_xMn_2O_4$ cathodes, where x was varied electrochemically from "zero" to 2.4. The observed infrared absorption peaks can be assigned to the various Mn-O and Li-O environments within the spinel framework. The results correlate well with XRD and neutron diffraction analyses in the literature as well as with the phase behavior indicated by electrochemical measurements. The technique gives both qualitative and quantitative information and is shown to be an effective companion technique to x-ray diffraction. The mechanisms responsible for capacity fading during normal cycling of $LiMn_2O_4$ cells in both the 3 V and 4 V regions were determined by examination of spectra obtained from electrodes following 25 cycles at charge and discharge rates of C/6. In the 3 V region, electroactive material becomes electronically disconnected from the rest of the electrode possibly due to fracture of the oxide particles during the cubic-to-tetragonal phase transformation. In the 4 V region, the active electrode material is gradually converted to a lower-voltage defect spinel phase *via* dissolution of manganese in the electrolyte.

Electrochemical properties of the metal oxide films, such as electrocatalyst kinetics, film corrosion behavior and active species diffusivity, can be measured by employing standard techniques for geometries with well-defined electrode-electrolyte interfaces. The pulsed laser deposition technique has been used to prepare smooth dense films $La_{0.6}Ca_{0.4}CoO_3$, $La_{0.6}Ca_{0.4}MnO_3$, $La_{0.5}Sr_{0.5}FeO_3$, $Bi_2Ru_2O_7$, $Li_xMn_2O_4$ and Li_xCoO_2 on substrates of stainless steel, quartz and silicon. High-quality crystalline films of all of the oxides except $Bi_2Ru_2O_7$ were obtained by deposition onto stainless steel at 600°C in the presence of 100 mtorr of O_2. The correct structure for the $Bi_2Ru_2O_7$ films was obtained by lowering the O_2 pressure while maintaining the total pressure with Ar.

The rates of O_2 reduction and evolution on thin films of $La_{0.6}Ca_{0.4}CoO_3$, $La_{0.6}Ca_{0.4}MnO_3$ and $La_{0.5}Sr_{0.5}FeO_3$, were measured with the RRDE technique in 0.1M KOH. The order of activity was $La_{0.6}Ca_{0.4}MnO_3$ > $La_{0.5}Sr_{0.5}FeO_3$ > $La_{0.6}Ca_{0.4}CoO_3$ with Tafel slopes of ~90 mV/decade. The order of activity for O_2 evolution was $La_{0.6}Ca_{0.4}MnO_3$ > $La_{0.6}Ca0.4CoO_3$ > $La_{0.5}Sr_{0.5}FeO_3$ with Tafel slopes of ~60 mV/decade. A partially carbon-coated $La_{0.6}Ca_{0.4}CoO_3$ film showed higher currents for O_2 reduction than the bare film, due to O_2 reduction on the carbon and further reaction on the neighboring $La_{0.6}Ca_{0.4}CoO_3$. We believe that

*Materials Sciences Division, LBNL

this is the first direct measurement of the synergism between O_2 reduction of the oxide and the carbon.

Films of $Li_xMn_2O_4$ and Li_xCoO_2 from 0.125 to 1.5 μm thick have been subjected to a wide range of electrochemical studies. Film capacity densities as high 56 and 62 mAh/cm²-μm were measured for $Li_xMn_2O_4$ and Li_xCoO_2, respectively. $Li_xMn_2O_4$ films have been subjected to >350 cycles at 10 mA/cm² with insignificant fading of capacity. Capacity losses on increasing charge and discharge current density to 100 mA/cm² were ~54%. These studies are not yet complete but they illustrate the promise of pulsed laser deposition for the production of cathode films for rechargeable lithium microbatteries.

The chemical diffusivities of lithium in $Li_xMn_2O_4$ were measured with the current step/relaxation technique with both thin-film and porous PTFE-bonded electrodes of $Li_xMn_2O_4$. Diffusion coefficients of 1-3 × 10^{-11} cm²/sec were measured in both electrodes if the critical distance in the porous electrode is assumed to be the grain size of the oxide as determined with x-ray diffraction, as opposed to the thickness of the electrode.

Future work will involve preparation and characterization of doped $Li_xMn_2O_4$ films. Extension of the FTIR techniques developed so far to investigations of thin-film electrode should yield further insight into capacity-fade mechanisms.

References

Striebel KA, Deng CZ, Cairns EJ. Pulsed laser deposition of transition-metal oxides for secondary batteries. *Materials Research Society Symposium Proceedings Series*, Vol. 393, Spring Meeting, Boston, MA, 1995.

Striebel KA, Deng CZ, Cairns EJ. Oxygen reduction on $La_{0.6}Ca_{0.4}CoO_3$ and $La_{0.6}Ca_{0.4}MnO_3$ thin films in alkaline electrolytes. Abs. No. 930, 188th Meeting of the Electrochemical Society, Chicago, IL, Vol. 95-2, October 1995.

Striebel KA, Deng CZ, Cairns EJ. Electrochemical behavior of $LiMn_2O_4$ and $LiCoO_2$ thin films produced with pulsed laser deposition. Submitted to *J. Electrochem. Soc.*, August 1995.

Wen SJ, Richardson TJ, Ma L, Striebel KA, Ross PN, Cairns EJ. FTIR spectroscopy of metal oxide insertion electrodes: capacity fading in secondary Li/$LiMn_2O_4$ cells. Submitted to *J. Electrochem. Soc.*, November 1995.

Wen SJ, Richardson TJ, Ma L, Ghantous DI, Striebel KA, Ross PN, Cairns EJ. Application of FTIR spectroscopy to the study of $LixMn_2O_4$ for rechargeable lithium batteries. Submitted to *J. Electrochem. Soc.*, December 1995.

Zinc/Nickel Oxide Batteries for Electric Vehicle Applications

T.C. Adler, F.R. McLarnon, and E.J. Cairns

The rechargeable alkaline Zn/NiOOH cell has the potential to meet all of the mid-term requirements for electric vehicle (EV) batteries established by the U.S. Advanced Battery Consortium (USABC). Compared to other rechargeable alkaline batteries such as Cd/NiOOH (nickel/cadmium) and MH/NiOOH (nickel/metal hydride), the Zn/NiOOH cell will have higher specific energy and lower cost. The lifetime of earlier versions of the Zn/NiOOH cell has been limited to 100-200 deep cycles because of the high Zn species solubility in alkaline electrolytes and consequent rapid redistribution of Zn electrode active material (shape change). In 1991 LBNL developed new electrolyte compositions which reduced zinc species solubility and eliminated the shape-change problem, thereby leaving the Zn electrode nearly unchanged after hundreds of cycles. Many life-cycle experiments with various electrolyte compositions indicated that 4.5 M KOH, 1.8 M KF and 1.8 M K_2CO_3 is near-optimal. LBNL 1.5-Ah Zn/NiOOH cells with this electrolyte typically retain >80% of their initial capacity for ~400 deep-discharge cycles, and >60% after ~550 deep-discharge cycles. This optimal cell operates well in a sealed, nearly maintenance-free mode and is tolerant of overcharge and overdischarge.

LBNL has entered into a CRADA with Energy Research Corporation (ERC) of Danbury, CT, to further develop Zn/NiOOH cells. Objectives are to scale-up the LBNL 1.5-Ah laboratory cell to 15-Ah and 150-Ah sizes, to more closely simulate EV batteries. ERC fabricated 15-Ah cells and delivered them to LBNL, where they passed USABC mid-term EV power tests. LBNL also evaluated several 1.5-Ah Zn/NiOOH cell configurations using ERC materials and proposed design modifications for ERC 15-Ah cells. One of these modifications, a change in separator configuration, produced a substantial improvement in the performance of ERC 15-Ah cells. ERC demonstrated long lifetimes (>300 deep charge-discharge cycles with <10% capacity degradation) with 15-Ah Zn/NiOOH cells containing the LBNL electrolytes in combination with improved low-solubility Zn electrodes developed by ERC. This important result not only confirms the beneficial effects of low-Zn-solubility electrolytes and electrodes, but also demonstrates the ability to scale up to larger cells.

Two problem areas were identified that delayed our plan to fabricate 150-Ah cells. First, lighter NiOOH electrodes are needed to achieve a specific energy that would provide an acceptable EV driving range. Second, dehydration of the NiOOH electrodes was observed to compromise cell performance after hundreds of cycles. One approach now under investigation is the establishment of an internal wicking mechanism within the NiOOH electrode that will not only hydrate the electrode for longer periods, but also reduce the mass of external wicking material. Another approach is to evaluate new lightweight microfiber nickel current collector materials.

High-Rate Zinc/Air Batteries for Consumer Applications

K. Striebel, S. J. Wen, J. Rheaume, and E.J. Cairns

LBNL is working with Rayovac Corp., using proprietary technology from both parties, on the development of high-rate single-use Zn/air batteries for consumer applications. Baseline performance of the Rayovac air electrode has been established in half-cell studies at LBNL. Several novel methods to reduce the kinetic overpotential of the electrode are under evaluation.

Future work will include application of electrolyte optimization techniques developed at LBNL under DOE support.

Applied Research on Lithium/Polymer-Electrolyte Cells

E.J. Cairns, Y. Chen, T. Devine, Z. Deng, M. Doeff, J. Evans, D. Ghantous, J. Kerr, F. Kong, K. Kinoshita, F.R. McLarnon, J.S. Newman, L. Rao, T. Richardson*, P.N. Ross*, K.A. Striebel, M. Tian, and S.-J. Wen*

LBNL and the U.S. Advanced Battery Consortium have completed work under a Cooperative Research and Development Agreement (CRADA) to advance Li/polymer-electrolyte battery technology. Investigators from both the Energy and Environment Division and the Materials Sciences Division participated in this effort. Research tasks included study of electrochemical phenomena at electrode/polymer electrolyte interfaces, development of advanced mathematical models of Li/polymer-electrolyte cells, synthesis of improved polymer electrolytes and materials for positive electrodes, establishment of an extensive bibliographic database on components for Li/polymer-electrolyte cells, an investigation of overcharge/overdischarge phenomena in secondary Li cells, and a study of corrosion processes in these cells.

*Materials Sciences Division, LBNL

Chemical Applications

Use of Limestone for Hot-Gas Cleanup and for Regeneration of the CaS Produced

M.W. Brooks, L.A. Fenouil, and S. Lynn

The development of reliable methods for removing solid and gaseous contaminants from coal-gas at high temperatures and pressures is one of the most important technological advances required in the field of coal gasification. Gaseous contaminants include H_2S, NH_3, and volatilized metal and alkali salts, all formed from trace components of the coal. Entrained solids are mainly gasifier fines formed during the gasification process. It is necessary that all of these be removed prior to the combustion of the coal gas to prevent damage to turbine equipment and infringement of emissions legislation.

This project explores the technical and economic feasibility of a high-temperature process for cleaning coal gas prior to combustion in a gas turbine. In the proposed process the coal gas would pass through a nearly isothermal, moving bed of millimeter-size calcium carbonate (limestone) particles that would serve to remove particulates (by filtration), hydrogen sulfide (by chemisorption), and ammonia (by catalysis). Other configurations, such as entrained-flow, fluidized and packed-bed sorption systems, have also been modeled. The objective of this research is to define the temperature at which these goals (mainly the sulfur removal) can best be realized at a given pressure and for a given coal gas composition, as well as to determine the performance of such a clean-up system. A further objective is to synthesize a process suitable for recovering the sulfur from the CaS formed in the process.

Study of Calcium-Based Sorbents Under Simulated Coal Gases

Thermodynamics

At a given fugacity of CO_2, limestone also undergoes calcination if the temperature is high enough (approximately 900°C for 1 bar of CO_2):

$$CaCO_3 \leftrightarrow CaO + CO_2 \quad (1)$$

Below the calcination temperature of limestone the desulfurization reaction of importance is:

$$CaCO_3 + H_2S \leftrightarrow CaS + H_2O + CO_2 \quad (2)$$

which becomes increasingly favorable as the temperatures increases. Above the calcination temperature of $CaCO_3$, the lime (CaO) formed can then react with H_2S:

$$CaO + H_2S \leftrightarrow CaS + H_2O \quad (3)$$

Reaction 2 is endothermic (about 165 kJ/mol at 900°C) whereas reaction 3 is exothermic (about 65 kJ/mol at 900°C). The lowest level of H_2S thermodynamically possible in a coal gas in contact with lime(stone) is obtained at the calcination temperature of the limestone, which is only a function of the partial pressure (*i.e.*, fugacity) of CO_2. However, it is favorable to operate the H_2S sorption reaction slightly above this temperature because of kinetic considerations (Fenouil and Lynn, 1995a,b). Extensive thermodynamic calculations show that the level of removal of H_2S could be well above the 90% mandated by the Clean Air Act. Figure 1 shows the value of the equilibrium H_2S level as a function of temperature for a typical gasifier pressure and gas composition.

Kinetics

All experiments were carried out with a differential tube reactor originally designed by Towler and described by Fenouil *et al.* (1994). The conversion of $CaCO_3$ to CaO and CaS and of $MgCO_3$ to MgO was followed by a combination of gravimetric measurements and of iodometric titrations of CaS (Fenouil, 1995).

Results for H_2S Sorption with Limestone

Sorbent choice

The H_2S-sorption capabilities of 18-35 mesh particles (average mass-radius of 0.40 mm) of three different calcium-based sorbents (limestone, $CaCO_3$; dolomitic limestone, $[MgCO_3\text{-}CaCO_3]_1[CaCO_3]_3$; dolomite $MgCO_3\text{-}CaCO_3$) were tested under simulated coal gases. Two fundamentally different behaviors were observed. Above the calcination temperature of $CaCO_3$, complete conversion of

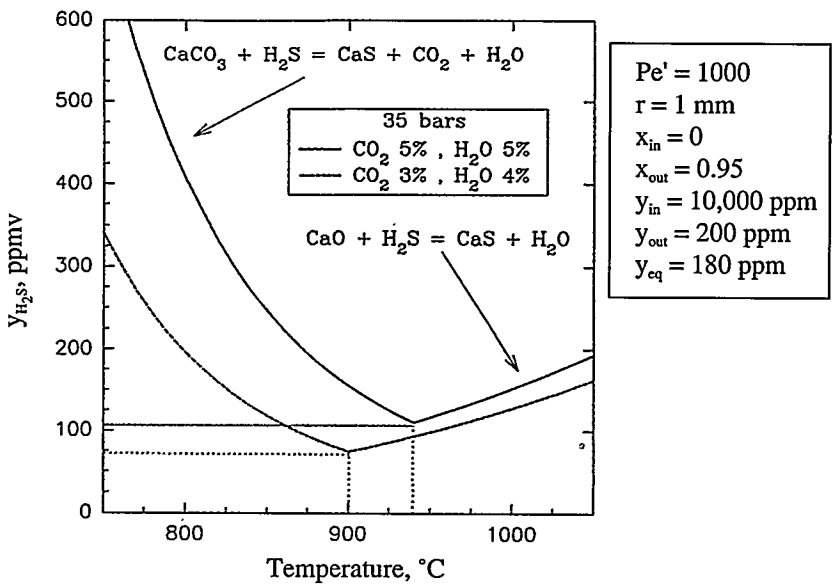

Figure 1. *Effect of temperature, CO_2 and H_2O on H_2S sorption by limestone ($Da' = \infty$).*

$CaCO_3$ to CaS can be achieved with all three sorbents (Fenouil and Lynn, 1995a). However, chemical attrition of the sorbent also increases as more magnesium is present. This chemical attrition, caused by near-explosive calcination of $MgCO_3$, is responsible for the formation of a relatively large quantity of fine powder. It thus appears that low-magnesium limestone, which has the best sulfur loading, should be the sorbent of choice. Nonetheless, dolomitic limestone and dolomite can also be used.

Below the calcination temperature of $CaCO_3$ (about 900°C under 1 bar of CO_2), less than 20% of the $CaCO_3$ in the limestone can be converted to CaS compared to 100% for dolomite. For the dolomitic limestone, all of the calcium atoms associated with the dolomite regions can be converted to CaS whereas only 20% of those associated with the limestone regions can be converted, yielding a maximum overall conversion of about 40%. Limestone is thus the preferred sorbent for coal-gas desulfurization, except at low temperatures (*i.e.*, below the temperature of calcination of $CaCO_3$) where only dolomites can be used effectively (Fenouil and Lynn, 1995a).

Kinetics of the reaction between H_2S and calcined limestone

Limestone particles can be completely converted to CaS when the temperature is held above the calcination temperature of the calcium carbonate. The reaction actually takes place between CaO and H_2S following a shrinking-core mechanism with a very sharp interface between the unreacted CaO core and the CaS product layer (Fenouil and Lynn, 1995c). When the temperature is higher than 20 to 30°C above the calcination temperature of $CaCO_3$, the kinetics of limestone calcination (reaction 2) becomes faster than that of lime sulfidation (reaction 3) and does not interfere with the overall sulfidation kinetics. The kinetics of the sorption of H_2S by CaO does not decrease significantly when the CaO is severely sintered for several hours at 1050°C prior to sulfidation. The CaS layer that forms on CaO appears to be much more permeable than that formed on $CaCO_3$, and conversion of millimeter-sized particles of CaO to CaS is complete in one to two hours if the H_2S concentration in the gas phase is maintained around 1%. Once CaO is formed, the reaction between CaO and H_2S is controlled by the diffusion of H_2S through the pores of the CaS product layer.

Design of the coal-gas cleanup system

Design equations describing fixed beds as well as co-current and counter-current moving beds of limestone particles sorbing H_2S (for plug-flow for gas and solid phase) have been developed and analytically solved for steady-state operation (or for constant-pattern breakthrough in the case of a fixed bed) using the Grain Model to describe the reaction kinetics (Fenouil and Lynn, 1996).

The concentration profile of H_2S and CaS along the bed length as well as the degree of utilization of the sorbent, the degree of removal of H_2S from the gas and the required bed total length can be expressed as a function of only five parameters: R, the radius of the limestone particles; y_{eq}, the thermodynamic equilibrium mole fraction of H_2S in the gas under bed conditions; $Sh' = 2(t_1+t_2)/t_3$, a modified Sherwood number (or Biot number); $Pe' = 6(t_1+t_2)/t_5$, a modified Péclet number (t_5 is a characteristic flow time, equal to $(R(1-e)r_S)/(u_G(C-C_{eq}))$ in the case of a fixed or moving bed, u_G being the superficial velocity of the gas); and $Da' = 6(t_1+t_2)/t_4$, a modified Damköhler number.

Figure 2 provides an example of the H_2S concentration profile as a function of the bed length for counter-current gas/solid flow in a moving bed (limestone particles of 2 mm diameter, 95% sorbent utilization, 98% sulfur removal (y_{out} = 200 ppm, y_{eq} = 180 ppm)). Using the kinetic data described in the preceding section and reasonable estimates of the operating conditions of a moving bed of limestone particles (*i.e.*, Pe' on the order of 1000, Sh' on the order of 200, Da' being extremely large), the total bed length is found to be of the order of 1 meter. For entrained-flow and fluidized-bed sorption systems, the gas/solid contact time should be of the order of one second.

Recovery of H_2S and $CaCO_3$ from CaS

A process studied by Keairns, *et al* (1974) is the reverse reaction of the sulfidation of calcium carbonate:

$$CaS + H_2O + CO_2 \rightarrow CaCO_3 + H_2S \quad (4)$$

This approach was found to be unsatisfactory because of the decrease in regenerability of the CaS as the number of cycles increased. Keairns reported that after 21 cycles the amount of CaS which could be converted to $CaCO_3$ decreased from 69 to 13%. Sintering was blamed for the regeneration difficulties. The argument could be made that the cost of lime is so small there is no need to regenerate the sorbent. This may be the case, but CaS is considered hazardous and its disposal must be preceded by oxidation to inert $CaSO_4$. Schwerdtfeger and Barin (1993) studied this process exhaustively but concluded that with a single-step process it was not possible to convert CaS quantitatively to $CaSO_4$.

The production of fresh $CaCO_3$ crystals from an aqueous slurry of CaS would eliminate crystal-structure problems that hindered gas-solid regeneration schemes. The formation of $CaCO_3$ by the reaction between CO_2 and solid CaS particles suspended in water was observed by Bechamp as early as 1869 (Gmelin, 1957). The reaction is identical to reaction (3)

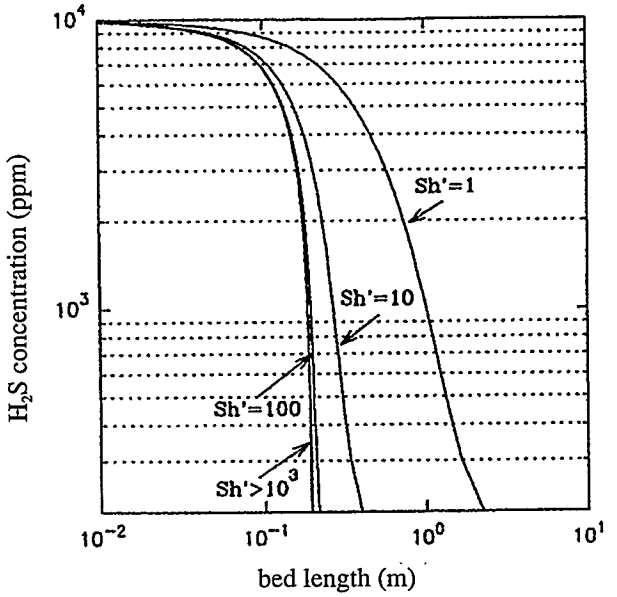

Figure 2. *H_2S Concentration as function of bed length for countercurrent flow configuration.*

except that it occurs in an aqueous solution. However, the reaction was incomplete due to the formation of a $CaCO_3$ layer around the CaS. Both CO_2 and CaS have low aqueous solubilities. The reaction between the aqueous CO_2 and solid CaS occurs between the dissolved CO_2 and solid CaS at the liquid-solid interface and is limited by how fast the CO_2 can dissolve and diffuse. The production of $CaCO_3$ at this interface eventually encapsulates the remaining CaS, preventing further reaction. Biswas and Dutta (1976) achieved 98% carbonation of 150 μm CaS particles in an aqueous slurry by controlling the CO_2 flow rate and bubble size. This carbonation was achieved with roughly three times the stoichiometric amount of CO_2, showing that high conversions of CaS are possible if the particle size is reduced enough.

An alternative is to reverse the reaction order as follows.

$$CaS + H_2S \rightarrow Ca(HS)_2 \quad (5)$$

$$Ca(HS)_2 + CO_2 + H_2O \rightarrow CaCO_3 + 2\,H_2S \quad (6)$$

An initial concentration of aqueous H_2S would react with CaS to form the highly soluble $Ca(HS)_2$ in one reactor, which then reacts in solution with CO_2 in a second reactor to precipitate $CaCO_3$ and produce more H_2S. The H_2S then reacts with CaS in the first reactor to perpetuate the reaction. The feasibility of such a reaction sequence would require a substantial increase in the aqueous solubilities of H_2S and CO_2. This can be done through the use of a solution of methyldiethanolamine (MDEA) or other alkanolamine. The reactions are as follows:

$$MDEA{\cdot}H_2S + CaS \rightarrow MDEA + Ca(HS)_2 \quad (7)$$

$$MDEA{\cdot}CO_2 + MDEA + Ca(HS)_2 + H_2O \rightarrow 2\,MDEA{\cdot}H_2S + CaCO_3 \quad (8)$$

In reaction (7), MDEA has complexed H_2S, keeping it in solution and readily available for reaction with solid CaS. The products of this liquid-solid reaction are free MDEA and $Ca(HS)_2$, which is very soluble in water. Carbon dioxide, bound in solution by MDEA, then reacts with the aqueous $Ca(HS)_2$ to precipitate $CaCO_3$ and produce H_2S, which is complexed by the free MDEA. A portion of the MDEA·H_2S stream is then used to produce more $Ca(HS)_2$ via reaction (7) and the remaining portion is stripped to produce concentrated H_2S. The stripped H_2S would contain only a small amount of CO_2 and water vapor and may easily be converted to elemental sulfur *via* the Claus process. The free MDEA produced after stripping may then be reloaded with CO_2 in an absorber, with a combustion gas as the CO_2 source, and be recycled to react with $Ca(HS)_2$.

The process described above has many benefits when compared to other CaS-regeneration techniques:

1) A very concentrated stream of H_2S is generated after $CaCO_3$ precipitation. This can readily be converted to elemental sulfur via the well-known Claus process.

2) "Fresh" $CaCO_3$ is obtained after each regeneration cycle. This eliminates crystal structure problems such as sintering that are experienced in many high-temperature gas/solid reactions.

3) The increase in H_2S and CO_2 solubility due to the MDEA decreases reaction times and eliminates the need for a large excess of CO_2.

4) The formation of the highly soluble $Ca(HS)_2$ eliminates CaS encapsulation, resulting in higher CaS conversions.

Burns (1995) studied the critical steps in the process outlined above. The effect of CaS particle size and prior CaS oxidation on the kinetics of $Ca(HS)_2$ generation (reaction 7) was determined. It was found that smaller crystals react more rapidly, as would be expected, and that freshly formed CaS reacts very much faster than partially oxidized material. The precipitation of $CaCO_3$ from solution, reaction (8), was also studied. Varying the concentrations of CO_2 and $Ca(HS)_2$ had little effect on the size of the $CaCO_3$ crystals produced, which were quite uniformly 10 μm in diameter and nearly spherical. An excess of only 10% of the CO_2 stoichiometrically required was found to adequate for complete $Ca(HS)_2$ conversion, and the reaction is complete as soon as the solutions are mixed. These data were then used to design an entire process for the production of H_2S and $CaCO_3$ from CaS.

Conclusions

Limestone presents the advantage of being cheap, readily available and relatively safe to handle. It is also among the best in thermodynamic performance for H_2S removal from coal gas at and above 800°C, where zinc-based sorbents cannot be used. Furthermore, CaS can easily and economically be regenerated to $CaCO_3$ and H_2S by a low-temperature aqueous process, and elemental sulfur can subsequently be recovered. For all these reasons, limestone appears to be the most suitable sorbent for high-temperature coal-gas desulfurization.

References

Brooks MW. *Recovery of Hydrogen Sulfide and Calcium Carbonate from Waste Calcium Sulfide.* M.S. Thesis, Department of Chemical Engineering, University of California, Berkeley, 1995.

Fenouil LA. Kinetic and structural studies of the sulfidation of large particles of lime and limestone in coal gas. *Ph.D. dissertation.* University of California at Berkeley, 1995.

Fenouil LA, Lynn S. Study of calcium-based sorbents for high-temperature H_2S removal. 1. Kinetics of H_2S sorption by uncalcined limestone. *Ind. & Eng. Chem. Res.* 1995a; 34: 2324-2333.

Fenouil LA, Lynn S. Study of calcium-based sorbents for high-temperature H_2S removal. 2. Kinetics of H_2S sorption by calcined limestone. *Ind. & Eng. Chem. Res.* 1995b; 3: 2334-2342.

Fenouil LA, Lynn S. Study of calcium-based sorbents for high-temperature H_2S removal. 3. Comparison of calcium-based sorbents for coal gas desulfurization. *Ind. & Eng. Chem. Res.* 1995c; 34: 2343-2348.

Fenouil LA, Lynn S. The design of entrained-flow and moving-, packed-, and fluidized-bed sorption systems: grain-model kinetics for hot coal-gas desulfurization with limestone. *Ind. & Eng. Chem. Res.* 1996; 35 (in press).

Fenouil LA. Towler GP. Lynn S. Removal of H_2S from coal-gas using limestone: kinetic considerations. *Ind. Eng. Chem. Res.* 1994, 33(2): 265-272.

Other Literature Cited

Biswas SC, Sabharwal VP, Dutta BK. Hydrogen sulphide from reduced gypsum. *Fertilizer Technology* 1976; 13(4): 255-258.

Gmelins Handbuch der Anorganishen Chemie, Ca 8 [B] (Auflage Calcium), Verlag Chemie GMBH, Weinheim, 1957 p. 645.

Keairns DL. et *al;* Sulphur emission control with limestone/dolomite in advanced fossil fuel processing system. *Envir. Aspects of Fuel Conver. Technology,* St. Louis, MO, 1974.

Schwerdtfeger K, Barin I. Problems in hot desulfurization of coal gas with lime. Erdol *und Kohle-Erdgas-Petrochemie* 1993; 46(3): 103-110.

Szekely J, Evans JW, Sohn HY. *Gas Solid Reactions.* New York: Academic Press, 1976.

Separations by Reversible Chemical Complexation

C.J. King

Highly hydrophilic organic solutes, notably carboxylic acids, glycols, glycerol, sugars, lower alcohols and phenols, are difficult to remove from water, yet they are high-volume products typically manufactured in aqueous solution and also appear in waste streams from many different industries. Carboxylic acids, glycols and alcohols are the most promising products for large-scale manufacture from biomass by fermentation. Because of chemical specificity, separations based upon reversible chemical complexation are promising for these applications. Our research pursues that general area.

Recovery of Carboxylic Acids

Our research in this area has dealt with extraction and adsorption of carboxylic acids, primarily lactic, acetic, succinic and fumaric acids, by use of basic extractants and adsorbents, notably those with amine functionalities. We have measured and interpreted equilibria and have developed methods of regeneration.

We investigated regeneration of the amine-based solid polymeric sorbent, Dowex MWA-1 (Dow Chemical Co.), by solvent leaching. The degree of acid removal by leaching with various Lewis-base solvents correlates well with the Gutmann Donor Number (DN). An interesting and potentially useful result is that the equilibrium distribution of acetic acid between Dowex MWA-1 and pyridine is greatly affected by small amounts of water. In the absence of water, the distribution of the acid from the sorbent into the solvent increases substantially. This suggests a regeneration process for low-volatility sorbed carboxylic acids wherein co-adsorbed water is first removed by stripping, and then the carboxylic acid is leached into a dry basic organic solvent.

We have measured equilibria for simultaneous adsorption of mixed acids with basic sorbents. Mixed acids are often encountered in fermentation and in waste streams, and it is often desirable to isolate individual acids. Measurements of both batch equilibria and fixed-bed separation of mixed lactic and succinic acids at various values of pH agreed with predictions made on the basis of complexation constants derived from single-acid data. Using another approach, a mixture of acetic and lactic acids in aqueous solution was successfully fractionated by sorption of the two acids together onto Dowex MWA-1, followed by selective vaporization of acetic acid. Furthering the work on lactic and succinic acids, we have been working closely through a Technical Assistance Agreement with a commercial firm engaged in separation of glycerol, lactic acid and succinic acid and possibly also pyruvic and citric acids as byproducts obtained from fermentation ethanol plant stillage.

We carried out an experimental study of the selectivity obtained between lactic acid and glucose during extraction with the tertiary amine extractant Alamine 336 (Henkel Corp.) in various diluents and also during adsorption by Dowex MWA-1. High-precision liquid chromatography was required, since the depletions of glucose in solution are low. Selectivities between these two solutes are critically important, since glucose is the substrate for production of lactic acid by fermentation. Seemingly small levels of contamination of lactic acid by glucose cause discoloration, thereby causing the lactic acid product to be off specification. Very high selectivities in favor of lactic acid (glucose uptakes of only 0.05 mg/g fresh solvent) were found for extraction by 15% (w/w) Alamine 336 in 1-octanol. The uptake of glucose by the solid sorbent Dowex MWA-1 was higher, in the range 5-10 mg/g dry sorbent, because of swelling of the sorbent. However, the sorbent exhibits about ten times the capacity of the extractant/diluent mixture on a weight basis.

Recovery of Glycols by Ion-Pair Extraction

The complexation properties of the -OH group are similar to those of water, and hence the most effective routes found for selective removal of glycols from aqueous solution through complexation have been based upon steric properties of the glycol. Following work on reversible reaction of glycols with aldehydes to form relatively non-polar dioxolanes, we returned to studies of separation by complexation with boronate functionalities. The uptake of propylene glycol during extraction of the glycol by an Aliquat 336 (Rohm & Haas Corp.)-phenylboronate ion pair in 2-ethylhexanol diluent is greater than stoichiometric, *i.e.*, more than 1.0 mole of glycol per mole of the ion pair. Nuclear magnetic resonance (NMR) studies indicated that this phenomenon is probably attributable to the formation of reverse micelles. We also examined and interpreted the effect of the nature of the diluent (2-ethylhexanol, o-xylene, toluene, diisobutyl ketone) on the degree of glycol extraction.

Recovery of Sugars and Glycols by Carbon Adsorption

We initiated studies on the adsorption of sugars by activated carbons, following leads from earlier research showing high capacities, substantial degrees of reversibility and considerable variation from carbon to carbon in the adsorption of sugars by different activated carbons. It appears that the high capacities, the differences in capacity, and possibly also the differences in reversibility, reflect the chemical properties of the carbon surfaces.

To measure adsorption isotherms with precision, we developed a precise liquid-chromatography analytical technique for measuring concentrations of glucose and ethylene glycol in aqueous solutions. Measurements of isotherms with different carbons are underway. Future work will relate uptakes and reversibilities to various indicators of carbon surface chemical functionalities.

Recovery of Phenols by Carbon Adsorption

There are many industrial needs for recovery of phenols, with applications including petroleum refining, processing of coals, processing of aqueous effluents from coke ovens in the iron and steel industry, and manufacture of phenolic compounds and resins. Activated carbons are effective for removal of phenols from aqueous solutions, and are frequently used for wastewater treatment. However, reversibility and full product recovery are difficult to achieve. Earlier research in our group demonstrated that irreversibilities in adsorption of phenols onto carbons stem from oxidative coupling reactions, which are catalyzed by the carbon surface and lead to the formation of phenyl ether oligomers. We are carrying out research to characterize this phenomenon better, and to identify and confirm ways in which carbon adsorption can most effectively be used for reversible uptake of phenols, enabling complete or nearly complete product recovery. We have begun by measuring ad-

sorption isotherms of phenol onto different commercial carbons derived from a variety of starting materials. Among the factors that we study will be the method of activation of the carbon and various chemical characterizations of the carbon surface.

References

Tung LA, King CJ. Sorption and extraction of lactic and succinic acids at pH > pK_{a1}. I. Factors governing equilibria. *Ind. Eng. Chem. Research* 1994; 33: 3217-3223.

Tung LA, King CJ. Sorption and extraction of lactic and succinic acids at pH > pKa1. II. Regeneration and process Considerations. *Ind. Eng. Chem. Research* 1994; 33: 3224-3229.

Broekhuis RR, Lynn S, King CJ. Recovery of propylene glycol from dilute aqueous solutions via reversible reaction with aldehydes. *Ind. Eng. Chem. Research* 1994; 33: 3230-3237.

Reisinger H, King CJ. Extraction and sorption of acetic acid at pH above pK_a to form calcium magnesium acetate. *Ind. Eng. Chem. Research* 1995; 34: 845-852.

King CJ, Poole LJ. Carboxylic Acid Sorption Regeneration Process. United States Patent No. 5,412,126. May 2, 1995.

Broekhuis RR, Lynn S., King CJ. Recovery of propylene glycol from dilute aqueous solutions by reversible chemical complexation with organoboronates. Lawrence Berkeley National Laboratory Report No. LBL-36913, May 1995.

Dai Y, King CJ. *Modeling of Fermentation with Continuous Lactic Acid Removal by Extraction Utilizing Reversible Chemical Complexation.* Lawrence Berkeley National Laboratory Report No. LBL-37485, July 1995.

Dai Y, King CJ. *Approaches for Regeneration of Amione-Carboxylic Acid Extracts.* Lawrence Berkeley National Laboratory Report No. LBL-37486, July 1995.

Bioinorganic X-Ray Spectroscopy

S.P. Cramer, M.M. Grush, X. Wang, L. Miller, M.-A. Arrio, G. Peng, J. Chen, C.R. Randall, J. Christiansen, H. Wang, A. Froeschner

Hard x-ray absorption spectroscopy, especially Extended X-Ray Absorption Fine Structure (EXAFS), has long been a popular tool for determining the structure of metal sites in biological samples such as enzymes. The vast improvement in brightness for synchrotron radiation sources such as the Advanced Light Source (ALS) and the Advanced Photon Source will permit more difficult types of spectroscopy to be conducted on dilute biological samples. Our group is developing and using the methods of soft x-ray absorption, x-ray magnetic circular dichroism, and high-resolution x-ray fluorescence for studying dilute metals in biological samples.

XMCD

In 1995 we conducted our first soft x-ray and XMCD experiments at the ALS. We commissioned a new XMCD apparatus with a superconducting split-coil magnet, a He3-He4 dilution refrigerator, and a 30-element fluorescence detector. Preliminary indications are that XMCD experiments can now be conducted at ~100 milliKelvin, allowing use of relatively weak magnetic fields to spin polarize the sample. We are using this apparatus to examine mixed-valence Fe and Mn systems (Figure).

High-Resolution X-Ray Fluorescence

X-ray experiments were also done by group members at the Stanford Synchrotron Radiation Laboratory (SSRL), the National Synchrotron Light Source (NSLS), and the European Synchrotron Radiation Facility (ESRF).

References

Christiansen J, Tittsworth RC, Hales BJ, Cramer SP. Fe And Mo EXAFS of *Azotobacter vinelandii* nitrogenase in partially oxidized and singly reduced forms. *J. Am. Chem. Soc.* 1995; 117: 10017-10024.

Wang X, Randall CR, Peng G, Cramer SP. Spin-polarized and site-selective x-ray absorption—demonstration with Fe porphyrins and K-beta detection. *Chem. Phys. Lett.* 1995; 243: 469-473.

Grush MM, Christou G, Hamalainen K, Cramer SP. Site-selective XANES and EXAFS–a demonstration with manganese mixtures and mixed-valence complexe. *J. Am. Chem. Soc.* 1995; 117: 5895-5896.

Van Elp J, Peng G, Zhou Zh, Adams MWW, et al. Nickel L-edge x-ray absorption spectroscopy of *Pyrococcus furiosus* hydrogenase. *Inorg. Chem.* 1995; 34: 2501-2504.

Ralston CY, Chen J, Peng G, George S, et al. Biological x-ray spectroscopy on 3rd generation synchrotron radiation sources. *Physica B* 1995; 209: 203-208.

Peng G, van Elp J, Jang H, Que L, et al. L-

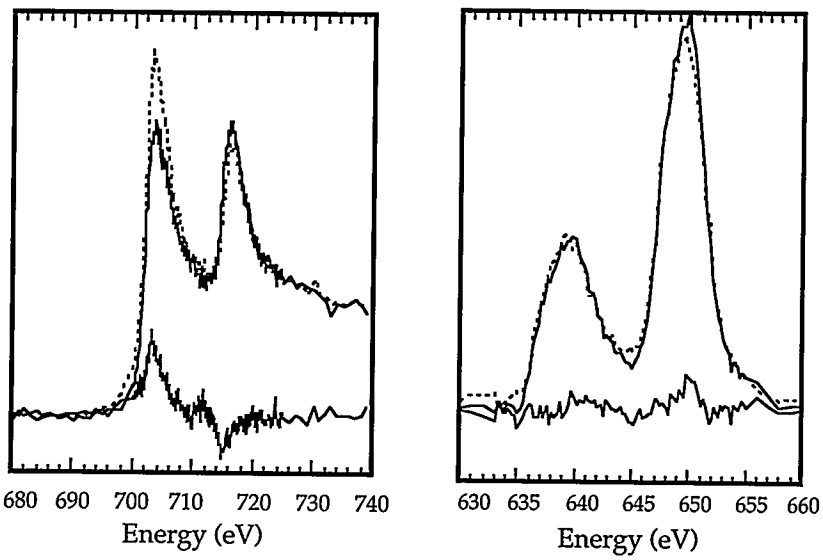

Figure. *Preliminary XMCD from ALS beamline 9.3.2. (Left) Fluorescence-detected absorption and XMCD for the Fe in purple acid phosphatase. (Right) XMCD for 450 $La_{0.8}Sr_{0.2}MnO_3$ film on $LaAlO_3$ substrate.*

edge x-ray absorption and x-ray magnetic circular dichroism of oxygen-bridged dinuclear iron complexes. *J. Am. Chem. Soc.* 1995; 117: 2515-2519.

Christiansen J, Peng G, Young AT, LaCroix LB, Solomon EI, Cramer SP. X-ray magnetic circular dichroism at temperatures < 1K: demonstration with the blue Cu site in plastocyanin. *Inorg. Chim. Acta* (in press, 1995).

Grush MM, Chen J, Stemmler TL, George SJ, Penner-Hahn JE, Christou G, Cramer SP. Manganese L-edge x-ray absorption spectroscopy of lactobacillus plantarum catalase and mixed valence manganese complexes. *J. Am. Chem. Soc.* (in press, 1995).

Cramer SP, Peng G, J Christiansen J, Chen J, van Elp J, George S, Young AT. Fluorescence detected soft XAS and MCD—applications to bioinorganic systems. In: *Proceedings of 11th International Conference on Vacuum Ultraviolet Radiation Physics* (in press, 1995).

Bioorganometallic Chemistry: The Reactions of (η^5-Pentamethylcyclopentadienyl)rhodium Aqua Complexes with Nucleobases, Nucleosides, Nucleotides, and Oligonucleotides

R.H. Fish, H. Chen, M.M. Olmstead, M.S. Eisen,† D.P. Smith, and S. Ogo*

Bioorganometallic chemistry is a relatively new aspect of metal-carbon bond compound reactivity that is focused on the reactions of organometallic aqua complexes with biological substrates in aqueous solution. We have been studying the reactions of nucleobases, nucleosides, nucleotides, and oligonucleotides in aqueous solution with Cp*Rh aqua complexes, as a function of pH. In this fiscal year, we demonstrated the rich and diverse structural chemistry uncovered *via* reaction of $[Cp^*Rh(H_2O)_2(OTf)_2]_x$ with 9-methyladenine, 1-methylcytosine, 9-ethylguanine, 9-methylhypoxanthine, 9-ethylhypoxanthine, adenosine, guanosine, adenosine and methyl-5'-adenosine monophosphates, and the oligos, dA_{2-4} and dA_{12}, at various pH values.

We have also discovered that supramolecular hosts, Cp*Rh cyclic trimer complexes, could form host-guest complexes with a number of biologically important guests. Moreover, we have also synthesized the first possible organometallic enzyme model, a two coordinate, 12-electron Rh(I) complex buried in a hyrophobic cavity of $[(Cp^*Rh)_2(\mu\text{-}OH)_3]^+$ dimers.

*Department of Chemistry, University of California, Davis, CA 95616.

†Department of Chemistry, Technion-Israel Institute of Technology, Haifa, 32000, Israel

References

Fish RH, Smith DP, Chen H, Maestre MF, Olmstead MM , Eisen MS, Haskel A. Bioorganometallic chemistry: The reactions of a (η^5-pentamethylcyclopentadienyl)rhodium aqua complex with nucleobases, nucleosides, nucleotides, and oligonucleotides. Chapter in: I. Horvath and F. Joo, eds. *Aqueous Organometallic Chemistry and Catalysis*. NATO ASI Series on High Technology, vol. 5. Kluwer Academic Publishers 1995; 259.

Chen H, Maestre MF, Fish RH. Bioorganometallic Chemistry. 5. Molecular Recognition of Aromatic Amino Acid Guests by Cp*Rh-Nucleobase/Nucleoside/Nucleotide Cyclic Trimer Hosts in Aqueous Solution *J. Am. Chem. Soc.* 1995; 117: 3631 and submitted to *J. Am. Chem. Soc.* 1996.

Eisen MS, Haskel A , Smith DP, Maestre MF, Fish RH. Aqueous organometallic chemistry: Structure and dynamics in the formation of (η^5-pentamethylcyclopentadienyl)rhodium aqua complexes as a function of pH. *Organometallics* 1995; 14: 2806.

Chen H, Olmstead MM, Smith DP, Maestre MF, Fish RH. Bioorgano-metallic chemistry. 6. The pH dependent synthesis and structural studies of monomer, dimer, and cyclic trimer complexes from the reactions of 9-methylhypoxanthine/9-ethyl-hypoxanthine nucleobases with (η^5-pentamethylcyclopentadienyl)-rhodium aqua complexes *Angew. Chem. Int. Ed. Engl.* 1995; 34: 1514.

Chen H, Olmstead MM, Maestre MF, Fish RH. Bioorganometallic chemistry. 7. A novel, linear, two-coordinate Rh(I) anionic amide complex formed by the reaction of the nucleobase, 1-methylthymine, with the $[(Cp^*Rh)_2(\mu\text{-}OH)_3]^+$ cation at pH 10: Molecular recognition an electrostatic interaction within an organometallic hydrophobic cavity. *J. Am. Chem. Soc.* 1995; 117: 9097.

Removal and Recovery of Toxic Metal Ions from Aqueous Waste Streams by Utilization of Polymer Pendant Ligands

R.H. Fish, S.-P. Huang, W. Li, J. Devenyi, K.J. Franz, E. Arnold, R. Giauque, and R. L. Albright

The purpose of this project is to investigate the use of polymer pendant ligand technology for the removal and recovery of economical and toxic metal ions from DOE waste streams. Polymer pendant ligands are organic ligands, bound to cross-linked, modified divinylbenzene-polystyrene beads, that are capable of selectively complexing metal ions. The metal ion removal step usually occurs through a complexation or ion exchange phenomena, and thus, recovery of the metal ions and reuse of the beads is readily accomplished.

The research objectives, which we have achieved this fiscal year, includes synthesis of selective polymer pendant ligands for removal and recovery of the metal ions of interest to the Efficient Separation and Processing Cross-Cutting Program goals, determination of rates of both removal and recovery of these metal ions, and transference of the technology to our industrial partner, AquaEss, San Jose, CA, for implementation of the polymer pendant ligand technology we have generated. The studies have initially focused on the waste waters of the Berkeley Pit (~pH = 2.5) located in Butte, Montana, with emphasis on the follow-

ing metal ions, Fe^{3+}, Al^{3+}, Cr^{3+}, Cu^{2+}, Zn^{2+}, Mn^{2+}, Mg^{2+}, Ni^{2+}, and Ag^{+}. Since Fe^{3+} was dominant in the Berkeley Pit waste waters, we placed special attention on devising Fe^{3+} selective polymer pendant ligands in order to be able to remove and recover the other economically important metal ions such as Cu^{2+}, Zn^{2+}, Mn^{2+}, Mg^{2+}, and Al^{3+}.

The removal and recovery of metal ions from aqueous waste streams is an area that will demand a considerable amount of attention for technology development. In addition to developing a wide range of technologies for specific metal ion removal and recovery applications, the tremendous advantage in having a generic based technology is that it can accommodate a wide range of applications with regard to metal ion and waste stream to be treated. Clearly, the cost effectiveness of the polymer pendant ligand technology would make it an excellent alternative to cumbersome precipitation techniques.

Accomplishments

The first priority for this task was to develop selective polymer pendant ligands for iron (Fe^{3+}) removal and recovery and our experimental studies at LBNL have successfully accomplished this aspect. The polymer pendant catechol ligand derivatives, sulfonated catechol, sulfonated 2-6-LICAMS, and sulfonated 3,3-LICAMS, were ideal biomimetic candidates for an Fe^{3+} selective polymer pendant ligand, since they are structurally similar to biological ligands that selectively sequester Fe^{3+} (Figure).

We have, therefore, been able to synthesize and evaluate the Fe^{3+} selectivity for the above-designated polymer pendant ligands. From pH values of 0.5 to 2.5, we have found that the following order for removal of Fe^{3+} from aqueous solution is as follows: 3,3-LICAMS >>>> CATS with high capacities (0.8 to 1 mmol/g beads) and excellent removal kinetic rates ($2\text{-}4 \times 10^{-4}$ sec^{-1}). Recovery of Fe^{3+} from the beads and then reuse of the beads was readily accomplished using a 2N H_2SO_4 solution.

In addition, the above designated polymer pendant ligands have been found to have utility in other DOE remediation problems, for example, selectively removing several radionuclides, Cs^{+} and Sr^{2+}, and environmentally important metal ions such as Hg^{2+} and Pb^{2+} from aqueous solutions. As well, we will also present data on several new polymer pendant ligand, PS-SED (Figure), that are highly selective to Ag^{+}, Hg^{2+}, Pb^{2+}, and Cd^{2+} for remediation of Resource Conservation and Recovery Act Metal Ions. Finally, synthesis of novel metal-ion templated polymers introduces a new concept for selective removal and recovery of metal ions from aqueous waste solutions.

References

Huang S-P, Li W, Franz K J, Albright RL, Fish RH. Polymer pendant ligand chemistry. 3. A biomimetic approach to metal ion removal and recovery from aqueous solutions with polymer-supported sulfonated catechol and linear catechol amide ligands. *Inorg. Chem.* 1995; 34: 2813.

Huang S-P, Franz KJ, Olmstead MM, Fish RH. Synthetic and structural studies of a linear bis-catechol amide, N, N'-bis(2,3-dihydroxybenzoyl)-1,7-diazaheptane (5-LICAM), and its complexes with Ni^{2+} and Co^{2+}: Utilization of a polymer supported, sulfonated analogue, 5-LICAMS, as a biomimetic ligand for divalent metal ion removal from aqueous solution. *Inorg. Chem.* 1995; 34: 2820.

Li W, Olmstead MM, Miggins D, Fish RH. Synthesis and structural studies of metal complexes of the biological ligand 2-quinaldic acid: Utilization of the polymer pendant analog, PS-2-QA, for selective aluminum ion removal from aqueous solution. *Inorg. Chem.* 1996; 35: 0000.

Li W, Coughlin M, Albright RL, Fish RH. Polymer pendant ligand chemistry. 4. Recovery of precious metal ions from strongly acidic solution with a polymer-supported o-phenylenediamine hydrochloride ligand. *Reactive Polymers* 1995; 28: 89.

Huang S-P, Devenyi J, Franz KJ, Arnold EH, Fish RH. Polymer pendant ligand chemistry. 5. The selective and competitive removal of Ag^{+}, Hg^{2+}, Cu^{2+}, Pb^{2+}, and Cd^{2+} ions from aqueous solution utilizing a novel N-sulfonylethylenebis(dithiocarbamate) ligand anchored on macroporous polystyrene-divinylbenzene beads. *Inorg. Chem.* 1996; 35: 51.

Patents

Fish RH. Sulfonated Catechol and Linear Catechol Amide Polymer Pendant Ligands for Removal and Recovery of Metal Ions from Aqueous Waste Streams. (in preparation by LBNL/DOE Patent Department, 1995).

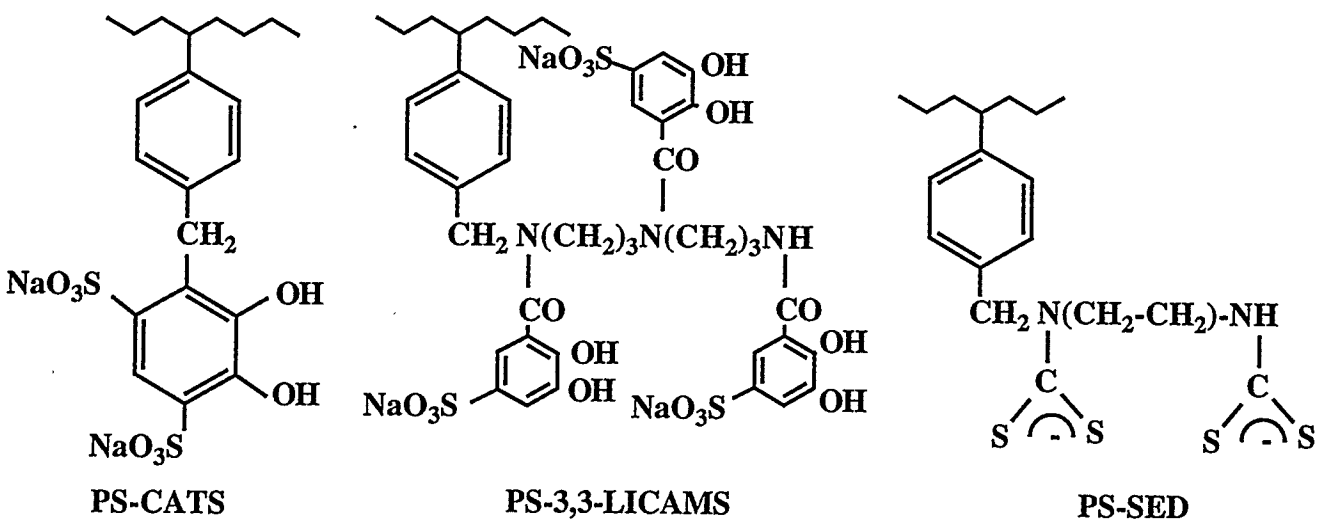

Figure. *Structural representations for three polymer pendant catechol ligand derivatives: PS-CATS, PS-3,3-LICAMS, and PS-SED.*

Mechanistic Aspects of the Oxidation of Alcohols and Alkanes with MMO Biomimics in Aqueous Solution and Aqueous Micelles

R.H. Fish, A. Rabion, R.M. Buchanan, S. Chen*, J. Wang*, and J.-L. Seris†*

The unique ability of water soluble methane monooxygenase enzymes (MMO) to oxidize a broad range of hydrocarbons has led to several environmental applications for the use of methanotrophic bacteria, including bioremediation of land contaminated by oil spills, and the oxidative removal of trichloroethylene from drinking water. Therefore, the utilization of biomimics of MMO in aqueous solution for the oxidation of water soluble substrates, such as alcohols, would be of interest from a mechanistic focus; previous MMO biomimetic oxidation studies have all been performed in organic solvents.

*Department of Chemistry, University of Louisville, Louisville, KY 40292

†Groupement de recherche de Lacq, BP 34, 64170 Artix, France

In this fiscal year, we studied the mechanisms involved in the oxidation of two water soluble substrates, cyclohexanol and benzyl alcohol, using several LFeOFeL complexes as catalysts with TBHP as oxidant in aqueous solution. Initial studies, on the mode of TBHP O-O bond scission, show dramatic effects of water on the mechanism of cleavage, and provide strong evidence for a homolytic scission of the peroxide bond (in acetonitrile the O-O bond scission mainly occurs *via* a heterolytic pathway to give Fe=O and t-BuOH) to provide t-BuO· radicals. *Thus, the t-BuO· radicals appear to be mainly responsible for the conversion of alcohol to ketone, not Fe=O complexes.* We also studied the oxidation of cyclohexane in aqueous micelles to provide a similar mechanism.

References

Rabion A, Chen S, Wang J, Buchanan RM, Seris J-L, Fish RH. Biomimetic oxidation studies. 9. Mechanistic aspects of the oxidation of alcohols with functional, active site methane monooxyenase enzyme models in Aqueous Solution. *J. Am. Chem. Soc.* 1995; 117: 12356.

Rabion A, Buchanan RM, Seris J-L, Fish RH. Biomimetic oxidation studies. 10. Cyclohexane oxidation reactions with active site methane monooxygenase enzyme models and t-butyl hydroperoxide in aqueous micelles: Mechanistic insites and the role of t-butoxy radicals in the C-H functionalization reaction. (submitted to *J. Molec. Catal.*, 1996).

Laser-Material Interactions

R.E. Russo, X.L. Mao, M. Kilgo, and S. Jeong

This report describes laser ablation as it is used with analytical spectroscopy for chemical analysis. The term *laser ablation* is used generically to describe the explosive *laser-material-interaction;* laser *sampling* refers to the removal of material from a solid using a pulsed laser beam with vapor transport to an analytical excitation source for analysis. Laser-material-interactions involve coupling of optical energy into a solid, resulting in vaporization, ejection of atoms, ions, molecular species, fragments, shock waves, plasma initiation and expansion, and a hybrid of these and other processes. Laser irradiance (power density) and the thermo-optical properties of the material are critical parameters that influence these processes.

Two general descriptions for the laser-material interaction are based on irradiance: *vaporization* and *ablation*. When the laser pulse duration is microseconds or longer and the irradiance is less than approximately 10^6 W/cm^2, vaporization is likely a dominant process influencing material removal. Although this interaction is defined as vaporization, the energy is delivered in a very short time and it is localized; thermodynamic models do not completely describe the interaction.

At higher irradiance, beyond 10^9 W/cm^2 with nanosecond and shorter laser pulses focused onto *any* material, an *explosion* occurs. The pressure over the irradiated surface from the recoil of vaporized material can be as high as 10^5 MPa (10^6 atmospheres). This explosive interaction has been described as "non-thermal," and melting is often not observed around the crater. During an ablative interaction, a plasma is initiated at the sample. Plasma temperatures are in excess of 10^4 K and radiative heat transport can establish a *plasma-material interaction.*

Laser Ablation and Atomic Emission Spectroscopy

Laser ablation is used for directly vaporizing solid samples for elemental analysis by the inductively coupled plasma (ICP) using atomic emission spectroscopy (AES). In turn, AES is used for studying laser ablation mechanisms. AES provides fundamental information on the laser plasma such as electron density, temperature, and temporal properties.

By transporting the sampled vapor to the ICP, we exploit additional capabilities of AES for studying laser ablation mechanisms. If the ICP conditions are constant, changes in the interaction due to laser parameters, inert gas environment, and material properties can be studied by observing elemental emission intensity in the ICP, temporally and spatially.

ICP-AES is probably the best technology for studying laser ablation at atmospheric pressure. AES is emphasized over mass spectrometry (ICP-MS) in our work to eliminate issues related to vacuum sampling from the atmospheric pressure ICP. However, ICP-MS would provide increased sensitivity for studying trace constituent behavior and fundamental properties such as the ablation threshold.

Laser Ablation Sampling for Analytical Spectroscopy

Laser ablation is the only technology that offers direct solid sampling from *any* material and *without* sample preparation. Sampling is initiated by optical absorption processes, thereby eliminating all restrictions on sample type, size, or geometry. Elimination of sample preparation is important, especially for haz-

ardous materials.

Another unique feature is that the diameter of the sampling area is measured in micrometers, allowing spatial analysis. With these advantages, however, laser ablation is not used widely, because the explosive laser material interaction is not fundamentally defined; it cannot easily be predicted or controlled. For unknown samples, it is impossible to know, *a priori*, how much sample will be ablated, or if the laser sampled material will be a stoichiometric representation of the solid.

The quantity of ablated sample and its composition depend on the laser and material characteristics. Fluctuations in the laser's temporal and spatial profiles, and non-linear power-density dependence contribute to this uncertainty. The sample's physical and chemical matrix will affect ablation behavior, and variations in the particle-size distribution of the ablated material will influence transport efficiency to the excitation source. This research involves several tasks to address these fundamental concerns.

A repetitively pulsed laser was determined to allow the sampled material from successive ablations to mix, providing *continuous* and/or *constant* ICP-AES signal response. Compared to single-pulse interaction, repetitive ablation provides better reproducibility for analysis, and a "controlled" environment for studying laser ablation mechanisms. Several capabilities beneficial to chemical analysis are immediately recognized from the improved precision. Optimization of the ICP for direct introduction of solids is possible during *constant* sampling. The power level to the ICP, gas flow rates and detection height can be varied to obtain the best signal-to-noise (S/N) and signal-to-background (S/B) ratios. Atom-formation processes in the ICP will be different during laser sampling than in liquid nebulization, and can be studied. Importantly, the excellent precision allows studies of ablation mechanisms as a function of laser properties, materials, and gas environments.

Roll-Off

For increased sensitivity, the laser power density can be changed to increase the quantity of sample delivered to the ICP. However, the efficiency of laser-energy coupling to the sample was found to change with power density, for both picosecond and nanosecond repetitive laser sampling. These roll-off studies lead to several important observations: the picosecond laser is more efficient than the nanosecond laser for removing sample, and the sample quantity (ICP-AES intensity) exhibits a strange power density dependence. The lower-energy picosecond provides higher ICP-AES intensity than the higher energy nanosecond laser, pointing out the importance of the energy deposition per unit time. For both lasers, the quantity of material increases with power density, but only up to a certain power density, at which point the quantity goes down. The plateau in intensity and *roll-off* (decrease) results from a change in the efficiency of laser energy coupling to the target by increased absorption and/or reflection from the laser-induced plasma, a process known as plasma shielding.

Similar behavior was observed for numerous samples, including metals, alloys, oxide insulators, and glasses. The roll-off occurs for all materials, for both picosecond and nanosecond sampling. Understanding plasma initiation and reducing plasma shielding is beneficial to the use of laser ablation for chemical analysis. Improved sampling efficiency as a function of laser power density can provide increased sensitivity in chemical analysis. Based on the above ICP-AES data, ultraviolet wavelengths were better than those in the infrared, and a picosecond pulse duration is better than is a nanosecond.

References

Russo RE. *Applied Spectroscopy* 1995; 49: 14A.

Mao XL, Russo RE. Thermal vaporization and inverse bremsstrahlung model to describe nanosecond plasma shielding. Presented at the Conference on Laser Ablation (COLA), EMRS meeting, Strasbourg, France, May 1995.

Mao XL, Shannon MA, Fernandez AJ, Russo RE. Temperature and emission spatial profiles of laser-induced plasmas during ablation using time-integrated emission spectroscopy. *Applied Spectroscopy* 1995; 49; 1054.

Fernandez AJ, Shannon MA, Mao XL, Russo RE. Correlation of spectral emission intensity in the inductively coupled plasma and laser-induced plasma during laser ablation of solid samples. *Analytical Chemistry* 1995; 67: 2444.

Shannon MA, Mao XL, Fernandez A, Chan WT, Russo RE. Laser ablation mass removal versus incident power density during solid sampling for inductively coupled plasma atomic emission spectroscopy. *Analytical Chemistry* 1995; 67: 4522.

Rostami AA, Greif R, Russo RE. Modified enthalpy method applied to rapid melting and solidification. *Int. J. Heat Mass Transfer* 1992; 35: 2161.

Chan WT, Russo RE. Study of laser material interactions using inductively coupled plasma atomic emission spectrometry. *Spectrochimica Acta* 1991; 46B: 1471.

Chan WT, Mao XL, Russo RE. Differential vaporization during laser ablation deposition of Bi-Sr-Ca-Cu-O superconducting materials. *Applied Spectroscopy* 1992; 46: 1025.

Mao XL, Chan W-T, Shannon MA, Russo RE. Plasma shielding during picosecond laser sampling of solid materials by ablation in He versus Ar atmosphere. *J. Appl. Phys.* 1993; 74: 4915.

Russo RE, Chan W-T, Bryant M, Kinard FJ. Laser ablation sampling with inductively coupled plasma atomic emission spectrometry for the analysios of prototypical glasses . *J. Anal. Atom. Spect.* 1995; 10: 295.

Chan WT, Russo RE. Characteristics of laser-material interactions monitored by inductively coupled plasma-atomic emission spectroscopy. In: J.C. Miller and R.F. Haglund, Jr., eds. *Laser Ablation Mechanisms and Applications.* Springer-Verlag 1991; 53-59.

Material Applications

Polarization-Dependent Measurements of Light Scattering in Sea Ice

A.J. Hunt, D. Miller and M.S. Quinby-Hunt

The goal of this research is to characterize the propagation and scattering of visible light in sea ice, to understand the connection between the light-scattering properties and ice morphology, and to evaluate the efficacy of polarimetry in optical remote-sensing studies of sea ice.

We are also developing a description of polarization-dependent light propagation and scattering in sea ice for modeling and interpreting remotely sensed data. Radiant transfer calculations in the ocean using scalar (non-polarization dependent) scattering have been shown to lead to large errors (~20%) in the radiance calculated using conventional scalar models. Scattering calculations are used to predict radiant transfer in sea ice and to evaluate effects of incident sunlight on climate change and on biological processes under the ice pack.

Because complete description of the angle- and polarization-dependent scattering of sea ice did not exist in the literature, we are measuring the polarized scattering properties of sea ice to characterize it and to identify relationships between the physical properties of the ice and polarization and scattering properties.

The scattering properties of sea ice are being characterized by *in situ* field measurements and extensive laboratory measurements on ice samples from cores gathered in Arctic seas and from artificial ice ponds. To perform the field measurements, we developed a bistatic, polarization-modulated nephelometer that analyzes the angle- and polarization-dependent light scattering in sea ice (Miller *et al.*, submitted to *Review of Scientific Instruments*). The instrument rests directly and noninvasively on the surface of the sea ice. (It can also be used to study scattering in snow and in sea water.) A visible laser beam (532 nm) is directed into the ice and the scattered light is detected by the analyzer optics. Both laser and detector angles can be varied.

This instrument was used to measure the angle- and polarization-dependent scattering in sea ice at Pt. Barrow, Alaska. Field measurements of the angle-dependent values of the first row (four elements) of the Mueller scattering matrix were made at sites in the Beaufort and Chukchi Seas during the EMPOSI field measurement program in the spring of 1994 using the bistatic polarization nephelometer. The results of these measurements corresponded to polarization information available from scattering from an unpolarized illumination source (sun).

To more completely characterize light scattering and propagation in sea ice an extensive series of laboratory measurements were performed at LBNL on samples obtained from various ice cores. The goal of these measurements was to measure the remaining twelve elements of the Mueller matrix, and to provide data over different and larger ranges of angles than was possible for the *in situ* measurements (instrument design constraints in the bistatic configuration limit its angular range). Additional goals of the measurements were to explore differences in ice types and the effects of orientation of the anisotropic sea ice samples on light scattering and propagation.

The existing laboratory polarization-modulated nephelometer was equipped with a cold stage and modified in other ways for ice measurements. Measurements were made of oriented first-year and multiyear sea ice taken from the Chukchi Sea near Point Barrow, Alaska. Samples of artificially grown saline ice from U.S. Army Cold Regions Research and Engineering Laboratory (CRREL) in Hanover, New Hampshire and liquefied sea ice were also examined. Samples were prepared various ways from ice cores, keeping careful track of orientation information. Thin-slab, cylinder, and square cross-section samples were fabricated with respect to the scattering geometry.

Although sea ice measurements vary significantly from sample to sample, several general conclusions can be drawn. The scattering intensity of thin slab samples of saline ice, oriented first-year ice, and multi-year ice all show very large forward and back scattering components and can be qualitatively described by scattering from pockets of brine with diameter ~30 mm in a medium of pure water ice. Results from thin slab samples from Point Barrow show a non-zero S_{12} which indicates a degree of linear polarization is induced by scattering in the ice. Phase functions for cylindrical samples do not exhibit the large forward and back scattering found in the thin slab samples and are generally featureless, implying the presence of multiple scattering.

Other results indicate that linear polarization is preserved in propagation through the ice and orientationally-dependent scattering. Orientation-dependent scattering effects are weakly manifested in thin slab c-axis oriented samples, and are evident primarily in the matrix elements S_{23} and S_{32}. This is consistent with a simple model that combines the effects of scattering from spherical inhomogeneities and the intrinsic birefringence of pure water ice. No orientational effects were observed for the cylindrical samples.

The major application of this work is to radiative transfer processes that occur within sea ice and to remote sensing. Direct sunlight entering sea ice at angles close to the horizon, which occurs in the Arctic, will have a partial degree of linear polarization due to refraction at high angles at the ice/air interface. The pres-

ence of polarization-dependent scattering in the sea ice samples observed suggests that vector radiance calculations will be useful to provide accurate radiant transfer predictions. Remote sensing of newly formed ice may detect orientation or alignment by the polarization of scattered light. Further work should address new and growing ice sheets to investigate this possibility.

References

Miller D, Quinby-Hunt, MS, Hunt AJ. Laboratory studies of the angle and polarization dependent light scattering in sea ice. (accepted for publication, *Applied Optics*)

Miller D, Quinby-Hunt MS, Hunt AJ. A novel bistatic polarization nephelometer for probing scattering through a planar interface. (submitted to *Review of Scientific Instruments*)

Hunt AJ, Miller D, Quinby-Hunt MS. Polarization properties of sea ice. Submitted to the National Meeting, Optical Society of America, Special Session on Scattering and Absorption in the Ocean, Portland Oregon, Sept. 10-15, 1995.

Aerogel Nanocomposite Materials

A.J. Hunt, M. Ayers, L. Erskine, M.S. Quinby-Hunt, X.Y. Song, P. Stevens, S.Q. Zeng

Aerogels form a class of porous, low-density, nanostructured solids with many unusual properties including very low thermal conductivity, high porosity, transparency, high surface area, catalytic activity, and low sound velocity. They have been fabricated with metal oxide, polymer, and carbon compositions. Silica aerogels have been investigated for use in superwindows, and as refrigerator and appliance insulation. Aerogels are prepared by sol-gel processing followed by supercritical extraction of the entrapped solvents. A Cooperative Research and Development Agreement (CRADA) was signed by LBNL and Aerojet Corporation to assist in achieving commercial production of silica aerogel.

Current research at LBNL involves developing new nanocomposite materials based on aerogel technology for a number of applications. Improving the thermal performance of aerogel, an important part of the research in recent years, has demonstrated that substantially improved thermal resistance can be achieved in aerogel insulation by adding a second phase to block the infrared component of heat transfer. This improved composite aerogel insulation operates at higher temperatures, provides a more compact insulation for space sensitive-applications, and lowers the final cost.

Superinsulating aerogel can replace existing CFC-containing polyurethane insulation, reduce heat losses in hot and cold piping, insulate batteries in electric vehicles, and reduce energy losses in a variety of industrial applications. We have also been exploring a much broader range of aerogel composite compositions using chemical deposition techniques. We have prepared many new composite aerogel materials with unusual properties attributable to their very fine dimensions (such as quantum-size effects). These materials may be useful for supercapacitors, sensors, electroluminescent displays, and other optical devices.

Thermal Insulation Research

The heat-transfer process in aerogel is more complex than in most other solids. Heat is transmitted by conduction through the solid phase, by the gas in the pores, and by radiation within the aerogel. Infrared radiation is responsible for half or more of the thermal conductivity in silica aerogel, depending on its temperature and the pressure of the gas it contains. Reducing the infrared radiant heat transfer substantially improves the thermal performance of aerogel insulation. At elevated temperatures (200 to 500°C), the radiative component of heat transfer in aerogel becomes dominant and must be suppressed. The infrared radiation can be blocked by adding a finely dispersed carbon with a high absorption coefficient.

We have developed and applied for a patent on a method using chemical vapor infiltration (CVI) to add carbon to aerogel that has advantages over older methods in which particle are added in the sol or liquid stage. Nanostructured aerogel composites materials can be created by using the catalytic decomposition of a gas inside the aerogel. This preparation method increases the strength of the aerogel and can provide much higher doping levels.

To characterize the carbon-doped nanocomposite materials prepared by the CVI method, infrared absorption and surface area were measured and High Resolution Electron Microscopy (HREM) was used to study the nanostructure. A Vacuum Insulation Conductivity Tester (VICTOR) was developed and used to measure the thermal conductivity of aerogel as a function of pressure and temperature. VICTOR was used to characterize doped and undoped aerogels. The best thermal performance of doped evacuated aerogels was about 4.5 mW/m/K (about ten times the thermal resistance of fiberglass insulation) and of nonevacuated doped aerogels was 13 mW/m/K.

To analyze and predict the thermal performance of aerogel the heat transfer due to the radiation, conduction, and gas conductivity and their interaction inside aerogel was modeled. The objective is to predict the thermal conductivity as a function of temperature and gas pressure for various doped and undoped aerogels. The predicted effects of carbon doping on the thermal performance of aerogel are significant at higher temperatures and if borne out, opacified aerogel will be an outstanding insulating material for industrial applications for temperatures up to 500°C.

Nanocomposite Aerogel Materials

We have explored a new family of unique nanoporous composite materials other than carbon based on CVI of aerogel. Nanophase aerogel composites were prepared with elemental silicon, iron, tungsten, and their oxides using the CVI process. Composites of silica aerogels and the oxides of iron, nickel, and copper were also synthesized using other techniques. Transmission electron microscopy was used to characterize the nanostructure and crystallinity of the new composites. Such nanophase materials have potential applications in ultra capacitors, batteries, and electroluminescent displays. Silicon-silica composites exhibit photoluminescence that we have confirmed arises from quantum well confinement effects. These materials may be useful for electroluminescent display devices.

Relatedly, we have developed a new method to treat aerogels with energetic gases to partly reduce silica to produce a material that exhibits photoluminescence. In this case, the photoluminescence is partly quenched by the presence of oxygen. We have developed a pressure/oxygen sensor based on this effect. A patent application covering the treatment process was filed in FY 1995.

References

Cao W, Hunt AJ. Sol-gel processing using organo-functional silanes. In: A.K. Cheetham, C.J. Brinker, M.L. Mecartney, and C. Sanchez, eds. *Better Ceramics Through Chemistry VI.* Pittsburgh: Materials Research Society 1994; 346; 631-636.

Hunt AJ, Ayers MR, Cao WQ. Aerogel composites using chemical vapor infiltration. *J. Non-Crystalline Solids* 1995; 185: 227-232.

Hunt AJ, Cao WQ. New routes to nanocomposite materials using aerogels. In: A.K. Cheetham, C.J. Brinker, M.L. Mecartney, and C. Sanchez, eds. *Better Ceramics Through Chemistry VI.* Pittsburgh: Materials Research Society 1994; 346: 451-455.

Lee D, Stevens PC, Zeng SQ, Hunt AJ. Thermal characterization of carbon opacified silica aerogels. *J. Non-Crystalline Solids* 1995; 186: 285-290.

Ludman JE, Ludman JJ, Callahan H, Caulfield J, Watt D, Sampson J, Robinson J, Davis S, Hunt AJ. Interferometeric atmospheric refractive-index environmental monitor. *Applied Optics* 1995; 34: 3267-3273.

Song XY, Cao W, Ayers MR, Hunt AJ. Carbon nanostructures in silica aerogel composites. *J. Materials Research* 1995; 10(2): 251-254.

Zeng SQ, Hunt AJ, Greif R, Cao WQ. Approximate formulation for coupled conduction and radiation rough a medium with arbitrary optical thickness. *J. Heat Transfer* 1995; 117: 797-799.

Zeng SQ, Hunt AJ, Greif R, Cao WQ. Mean free path and apparent thermal conductivity of a gas in a porous medium. *J. Heat Transfer* 1995; 117: 758-761.

Zeng SQ, Hunt AJ, Greif R. Transport properties of gas in silica aerogel. *Journal of Non-Crystalline Solids* (in press, 1995).

Zeng SQ, Hunt AJ, Greif R. Theoretical modeling of carbon content to minimize the heat transfer in silica aerogel. *J. Non-Crystalline Solids* 1995; 186: 271-277.

Zeng SQ, Hunt AJ. Mean free path and apparent thermal conductivity of gas in aerogel. Accepted for publication in *J. Heat Transfer* 1995.

Zeng SQ, Hunt AJ, Cao WQ, Greif R. Pore size stribution and apparent gfas thermal conductivity of silica aerogel. *J. Heat Transfer* 1994; 116: 756-759.

Zeng SQ, Hunt AJ, Greif R. Calculation of coupled conduction and radiation through an aerogel slab. Accepted for publication in *J. Heat Transfer.*

Zeng SQ, Hunt AJ, Greif R. Geometric structure and thermal conductivity of porous medium aerogel. (accepted for publication in *J. Heat Transfer*)

Ion-Assisted Pulsed Laser Deposition of High-Temperature Superconductor Thin-Film Structures

R.E. Russo, R.P. Reade, P. Ridgeway, and P. Berdahl

Most demonstrations of high-temperature-superconductor thin film structures have utilized single-crystal substrate materials. However, to extend the range of potential applications using these materials, we have developed technology to allow fabrication on amorphous and polycrystalline substrates.

One application for which this technology may prove appropriate is the high-temperature superconductor-based multichip module (MCM). MCM designs require several $YBa_2Cu_3O_{7-d}$ (YBCO) thin film layers in addition to low- and high-dielectric layers. The first layer is a superconducting ground plane, with several additional YBCO layers patterned as interconnects linking individual chips. Between the YBCO films, a relatively thick (~5 μm) low-dielectric layer is required.

Present HTSC MCM designs require all layers to maintain an epitaxial relationship throughout the multilayer structure, and large area expensive single crystal substrates are required. This requirement limits the choice of the dielectric material and the substrate, as both must be lattice matched to the YBCO crystalline structure. It is difficult to find materials with a low dielectric constant, proper coefficient of thermal expansion, and the appropriate lattice constant for multilayer YBCO structures. Thus, it would be practical to eliminate the need for epitaxy throughout the layers of a HTSC MCM, allowing the use of amorphous or polycrystalline dielectric materials and substrates.

The key to this technology is the development of an ion-assisted pulsed laser deposition (IAPLD) process to deposit biaxially-aligned yttria-stabilized zirconia (YSZ) intermediate layers on polycrystalline and amorphous substrates. We first demonstrated the deposition of such layers on Haynes Alloy #230 (HA230), a polycrystalline Ni-based superalloy. HA230 has a good coefficient-of-thermal-expansion match to YBCO, as well as strength, flexibility, and other properties suitable for HTSC tape conductors. Using the IAPLD YSZ intermediate layers, YBCO thin films of high critical current density (J_c) were deposited on HA230. The high J_c is attributable to the in-plane alignment (or "biaxial alignment") induced by the ion-assisted process, which minimizes detrimental high-angle grain boundaries in the subsequently deposited YBCO. In the current work, we demonstrate the IAPLD technology for eliminating the epitaxial requirement throughout a HTSC multilayer structure. In particular, we demonstrate the use of amorphous dielectric layers and amorphous and polycrystalline substrates in an HTSC MCM-type design.

For this study, SiO_2 was chosen as an amorphous dielectric layer material due to its low dielectric constant (ε~3.8) and widespread use in microelectronics. SiO_2 is an excellent low-dielectric material but may be difficult to use with YBCO, as the coefficients of thermal expansion are significantly different for these materials, leading to the potential for cracking in the films. In addition, a Pyrex-type glass was used as a substrate to demonstrate deposition on a common amorphous

substrate material.

The SiO_2 layers were deposited on three different substrates. First the SiO_2 was deposited in compression on the 1-μm-thick, randomly oriented polycrystalline HA230. Biaxially aligned YSZ intermediate layers were then deposited by IAPLD. Finally, YBCO was deposited *in situ* using the same conditions as in our previous work.

The second "substrates" utilized for this study are YBCO/CeO_2/YSZ samples obtained commercially from Conductus, Inc. These samples consist of a 0.2-μm YBCO thin film deposited epitaxially on a 2-inch single-crystal YSZ substrate with a thin CeO_2 buffer layer. We fabricated an additional multilayer structure on top of these samples, consisting of thin YSZ intermediate layers, a thick low-dielectric layer, and an additional YBCO layer. Before deposition of the SiO_2 thick layer, the samples were diced into 1-cm squares, and an ~ 0.1-μm YSZ layer was deposited by pulsed-laser deposition at 200°C and 1.0 mtorr oxygen pressure to protect the YBCO film from chemical interaction with the SiO_2. After the SiO_2 deposition and prior to the deposition of the IAPLD YSZ and second YBCO layers, the structure is SiO_2/YSZ/YBCO/CeO_2/YSZ. Finally, the third substrate utilized was the Pyrex-type glass, on which a YBCO/CeO_2/YSZ/Pyrex structure was fabricated.

The film thicknesses for the YBCO/YSZ/SiO_2/HA230 multilayer structure are approximately 0.4 μm YBCO, 0.2 μm YSZ, and 5 μm SiO_2. The YBCO film was highly *c*-axis oriented, as demonstrated by strong series of (00*l*) peaks in the x-ray diffraction. The superconducting transition temperature (T_c) of this film was ~87 K. A 50-μm-wide bridge was patterned for critical current density (J_c) measurements with and without a 0.4 T magnetic field. In the absence of magnetic field, the 77 K J_c is 3×10^5 A/cm². At 73 K in magnetic field, J_c is 7×10^3 and 2×10^3 A/cm² with field parallel and 45° to the film, respectively.

Preliminary results for the deposition of the YBCO/CeO_2/YSZ structure on Pyrex-type glass are also promising. An x-ray diffraction measurement of this multilayer (Figure) demonstrates successful deposition of a highly *c*-axis YBCO film on the (001)-oriented intermediate layers. The (T_c) of this film was ~87 K, and the J_c is approximately 10^4 A/cm². The J_c is believed to be limited by microcracks in the film formed during the process due to the heating of the substrate material to near its melting temperature. This problem may be reduced or eliminated by minor changes in the deposition parameters; further study is in progress.

The requirements of epitaxy throughout a HTSC multilayer structure can be eliminated when the IAPLD technology is employed to deposit a thin oriented intermediate layer. We have demonstrated the fabrication of structures that are suitable for application in multichip modules as well as high-current superconducting tapes. Further work is underway to study deposition parameters such as the achievable deposition rates and optimal film thicknesses.

References

Reade RP, Berdahl P, Russo RE, Schaper LW. Y-Ba-Cu-O multilayer structures with amorphous dielectric layers for multichip modules using ion-assisted pulsed-laser deposition. *Applied Physics Letters* 1995; 66: 2001-2003.

Reade RP, Berdahl P, Russo RE, Schaper LW. Multilayer Y-Ba-Cu-O structures using ion-assisted intermediate layers. *IEEE Transactions on Applied Superconductivity* 1995; 5: 2007-2010.

Reade RP, Church SR, Russo RE. Ion-assisted pulsed-laser deposition. *Review Of Scientific Instruments* 1995; 66: 3610-3614.

Reade RP, Berdahl P, Russo RE. Ion-assisted pulsed laser deposition of oxide thin films as templates for epitaxial-like growth of crystalline films on amorphous and polycrystalline substrates. Presented at Materials Research Society Fall Meeting, Bostom, MA, November 1995.

Russo RE, Mao XL, Perry DL. Pulsed laser deposition of thin films. *Chemtech* 1994; 24: 14-17.

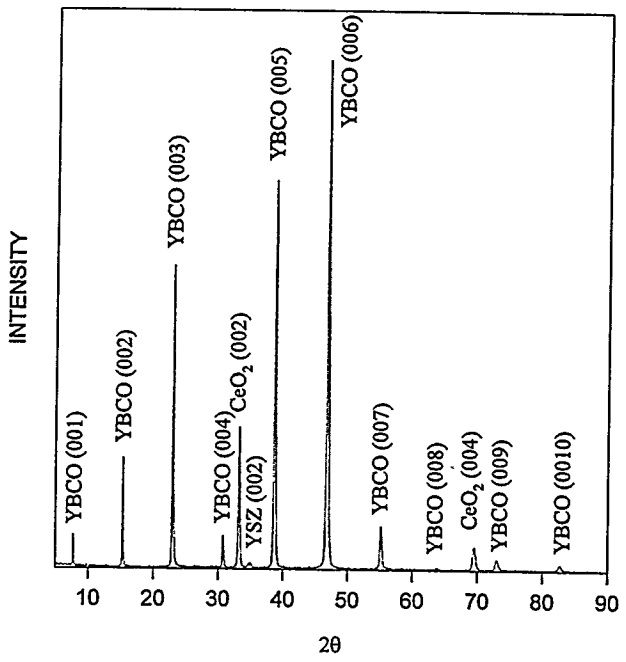

Figure. *X-ray diffraction pattern for a YBCO/CeO_2/YSZ Pyrex-type glass structure.*

Sponsors

Support from the following sources was provided through the U.S. Department of Energy under Contract No. DE-AC03-76SF00098:

U.S. Department of Energy, Assistant Secretary for Energy Efficiency and Renewable Energy:
Office of Transportation Technologies, Electric and Hybrid Propulsion Division
Office of Industrial Technologies, Office of Industrial Processes
Office of Industrial Technologies, Advanced Industrial Concepts Division, Advanced Industrial Concepts Materials Program

U.S. Department of Energy, Assistant Secretary for Environmental Management, Office of Technology Development, Office of Research and Development

U.S. Department of Energy, Office of Energy Research:
Office of Basic Energy Sciences, Chemical Sciences Division
Office of Health and Environmental Research, Medical Applications and Biophysical Research Division

Morgantown Energy Technology Center, Assistant Secretary for Fossil Energy, Office of Coal Utilization, Advanced Research and Technology Development, Division of Surface of Coal Gasification

Lawrence Livermore National Laboratory Contract No. W-7405-ENG-48

Office of Naval Research, Ocean, Atmosphere, and Space and Technology Department

United States Advanced Battery Consortium

Elf Aquitaine, Inc. (gift)